Received: 1 March 2019 | Revised: 5 November 2019 | Accepted: 17 December 2019

DOI: 10.1002/joc.6458

RESEARCH ARTICLE

International Journal of Climatology RMetS

NORA10EI: A revised regional atmosphere-wave hindcast for the North Sea, the Norwegian Sea and the Barents Sea

Hilde Haakenstad[1,2] | **Øyvind Breivik**[1,2] | **Magnar Reistad**[1] | **Ole J. Aarnes**[1]

[1]Norwegian Meteorological Institute, Bergen, Norway

[2]Geophysical Institute, University of Bergen, Bergen, Norway

Correspondence
Øyvind Breivik, Norwegian Meteorological Institute, Alleg 70, 5007 Bergen, Norway.
Email: oyvind.breivik@met.no

Funding information
ERA4CS, Grant/Award Number: WINDSURFER

Abstract

NORA10EI, a new atmosphere and wave hindcast for the Norwegian Sea, the North Sea and the Barents Sea is presented. The hindcast uses ERA-Interim as initial and boundary conditions and covers the period 1979–2017. The earlier NORA10 hindcast used ERA-40 as initial and boundary conditions before September 2002 and operational analyses from the European Centre for Medium-Range Weather Forecasts (ECMWF) in the continuation. This change in initial and boundary conditions may lead to non-stationarities in bias and random errors, and it is a question of some concern whether this also leads to spurious trends. We investigate this by comparing the two hindcasts. We find only minor differences in the statistics of means and upper percentiles, but somewhat larger differences in the extremes (100-year return values) of significant wave height and 10-m winds. Generally, NORA10EI outperforms NORA10 in the ERA-40 period (before September 2002) since ERA-Interim outperforms ERA-40. Conversely, NORA10 outperforms NORA10EI after 2006, since the operational ECMWF analyses here outperform ERA-Interim. Years 2002–2006 is a transition period with minor differences between the NORA10 and NORA10EI where the resolution of ERA-Interim is lower than that of the ECMWF analyses, but its physics are from a more recent model (2006). An important finding is that the regional hindcasts appear quite insensitive to changes in the host reanalysis with no statistically significant differences in mean and upper percentile trends of wind speed and wave height. A comparison of four polar low cases confirms that using ERA-Interim as host reanalysis yields a slightly better representation of evolution and intensity of polar lows than NORA10 in the ERA-40 period and the opposite after 2006.

KEYWORDS

North Sea, Norwegian Sea, regional hindcast, trend analysis, wave modelling

1 | INTRODUCTION

Regional downscaling of global reanalyses of the atmosphere and the wave field, known as hindcasts (a model run without data assimilation but constrained by a reanalysis on the boundaries and as initial conditions), are a cheap and useful supplement to regional reanalyses as they are affordable on much higher lateral resolution

without the need for an expensive data assimilation system. Several high-quality regional hindcasts have been generated in recent years (e.g., the studies by Gaslikova and Weisse, 2006; Weisse and Günther, 2007 and Weisse and von Storch, 2010 for the North Sea and the NORA10 hindcast by Reistad *et al*., 2011 to be investigated here). As waves are entirely forced by the wind, these studies perform well without assimilation of wave observations. Wave hindcasts are useful since the regional wave climate requires relatively high resolution to resolve topographical features that modify the wind field and obstruct the wave field. A number of regional (e.g., Bromirski *et al*., 2013; Izaguirre *et al*., 2013; Appendini *et al*., 2014; Semedo *et al*., 2015), basin-scale (Wang *et al*., 2012) and global (Semedo *et al*., 2011; Aarnes *et al*., 2015; Meucci *et al*., 2019) studies on wave climate variability and trends from hindcasts and reanalyses have recently been presented. Common to all of them is that they take their boundary conditions from global reanalyses.

The first global reanalyses were the ERA-15 reanalysis (Gibson *et al*., 1997) developed at the European Centre for Medium-Range Weather Forecasts (ECMWF) and the 40-year reanalysis (since extended) developed at the National Centers for Environmental Prediction/National Center for Atmospheric Research (NCEP/NCAR) (Kalnay *et al*., 1996). These were followed a few years later by the first coupled atmosphere-wave reanalysis, ERA-40 (Uppala *et al*., 2005), developed at ECMWF.

After ERA-40 came a series of global atmospheric reanalyses, most notably the Japanese Reanalysis (JRA-25, Onogi *et al*., 2007), the Climate and Forecast Reanalysis (CFSR, Saha *et al*., 2010), the Modern Era Reanalysis (MERRA, Rienecker *et al*., 2011), ERA-Interim (Dee *et al*., 2011), and the updated version of CFSR (CFSv2, Saha *et al*., 2014). Recently, century-long reanalyses have been produced at lower resolution, notably the 20th-century reanalysis, covering the period from 1871 to present (Compo *et al*., 2011) and ERA20C, covering the period 1900–2010 (Hersbach *et al*., 2015; Poli *et al*., 2016). The latter was recently accompanied by CERA20C, a coupled atmosphere–ocean low-resolution reanalysis (Buizza *et al*., 2018; Laloyaux, 2018).

ERA-Interim is continually updated but is not extended back beyond 1979. Compared with ERA-40, ERA-Interim has an improved hydrological cycle and better stratospheric circulation. Furthermore, in situ observations and satellite data are handled by four-dimensional variational data assimilation whereas ERA-40 employed a three-dimensional (3D) variational assimilation scheme (Dee *et al*., 2011). Although now being replaced by the new modern-era reanalysis ERA-5 (Hersbach and Dee, 2016), ERA-Interim is still used extensively.

NORA10 (Reistad *et al*., 2011) is a regional atmosphere and wave hindcast which employs ERA-40 on the boundaries and as initial conditions for the atmosphere, and spectra from a coarser wave model forced with ERA-40 winds for the wave field. NORA10 originally covered the same period as ERA-40, September 1957 to September 2002, but has since been extended to present time using operational analyses as boundary and initial conditions (Aarnes *et al*., 2012). (This extension is referred to as the second period of NORA10). Although of high quality, this inconsistency in the boundary forcing has led to concerns about the stationarity of the statistical properties of the hindcast archive since model upgrades have inevitably led to improvements and thus a reduction of bias and random error in the boundary and initial conditions. The question of whether the intensity of storm systems has been affected by these gradual changes to the forcing is of particular interest. This would show up as spurious trends which could also be interpreted as a climate change signal and compromises extreme value estimation (Aarnes *et al*., 2015). This question of how sensitive a regional hindcast is to its host analysis is of wider scientific interest, as reanalyses are often found to yield spurious trends due to increasing amounts of observations (of improving quality), see Aarnes *et al*. (2015) and Meucci *et al*. (2019).

In order to explore the stationarity issue, we have applied ERA-Interim on the boundaries of the NORA10 model domain and run the atmospheric model for the period 1979–2017. ERA-Interim was the best reanalysis available at the start of the NORA10EI production, and it is comparable in quality to the ECMWF analyses used for the early second period of the NORA10 hindcast.

The same wave model as was used for NORA10 was employed to produce wave fields for the period, where an outer wave model forced by ERA-Interim winds provided spectral wave boundary conditions to the inner model. With other things kept constant, we will thus investigate whether the change from ERA-40 to ECMWF analyses on the boundaries has led to spurious trends in mean and upper percentiles of the wind and wave field of NORA10.

This paper is organized as follows. A description of the new NORA10EI hindcast is presented in Section 2. A presentation of the general performance of NORA10EI follows in Section 3. Section 4 investigates median and upper percentiles of the wind speed at offshore wind-measuring stations. Section 5 assesses the performance of the wave model fields against offshore wave-measuring stations. The trends in wind speed are investigated in Section 6 and spatial wind patterns are presented in Section 7. A comparison of extreme value estimates from NORA10 and NORA10EI is presented in Section 8. The total impact of the transition to operational analyses on

NORA10 is discussed in Section 9 and the conclusions are summarized in Section 10. A short description of the usage of the offshore observations related to Section 4 is given in Appendix A1. Four polar low cases are presented in Appendix A2 (Figures A1–A8) where the relative merit of NORA10 v NORA10EI is considered, and the method used in trend analysis in Section 6 is presented in Appendix A3.

2 | MODEL SETUP

This hindcast study has deliberately been set up on the same model domain and with a configuration which closely matches that of NORA10. This is because we aim to investigate the sensitivity of a regional hindcast to host analysis forcing, and to what extent NORA10 is affected by the change in forcing data in 2002 where the transition from ERA-40 to ECMWF analyses takes place. The only exception to this is that the wind input to the wave model is hourly instead of 3 hr. This is not expected to have a major impact on the performance, except to give a slightly better representation of the upper percentiles.

The NORA10 atmosphere and wave hindcast (Reistad *et al.*, 2011) was based on an atmospheric downscaling of the global ERA-40 reanalysis (Uppala *et al.*, 2005). The wave model was set up in a nested configuration where ERA-40 10-m winds were used to force a 50-km resolution wave model covering the North Atlantic which provided boundary conditions for a 10-km wave model (see Breivik *et al.*, 2009 for details on the nesting scheme).

The NORA10EI atmospheric downscaling uses ERA-Interim as boundary and initial conditions but is otherwise, identical to NORA10. The HIgh-Resolution Limited Area Model (HIRLAM, see Unden *et al.*, 2002) is run in four 9-hr forecast sequences every day. HIRLAM is initialized by a blending of the ERA-Interim reanalysis and the previous HIRLAM forecast, valid at the start time of the forecast. This allows small scale structures to develop freely in the forecast while the large-scale structures are being controlled by the large-scale forcing Yang (2005).

The model domain is a rotated spherical grid with the south pole positioned at 22°S, 40°W (see Figure 1). The domain is 248 × 400 grid points with 0.1° resolution. The vertical is resolved by 40 hybrid levels with variable spacing. Near the surface, the vertical coordinate closely follows the terrain and it gradually transforms with height toward a pressure coordinate at the top of the domain. The model equations are solved by a semi-implicit, semi-Lagrangian two-time level integration scheme and the time step is 240 s (Unden *et al.*, 2002). Sequences of 10-m wind fields from +3 to +8 hr lead time exhibit the lowest biases and random errors and were therefore chosen for the wave model forcing as well as the model-observation comparison presented in the following sections.

No changes were made to the wave model physics or the spectral or spatial resolution. The WAM Cycle 4 model physics is described by Günther *et al.* (1992); Komen *et al.* (1994). The ice coverage was updated every 10 days based on the ice concentration in the ERA-Interim reanalysis.

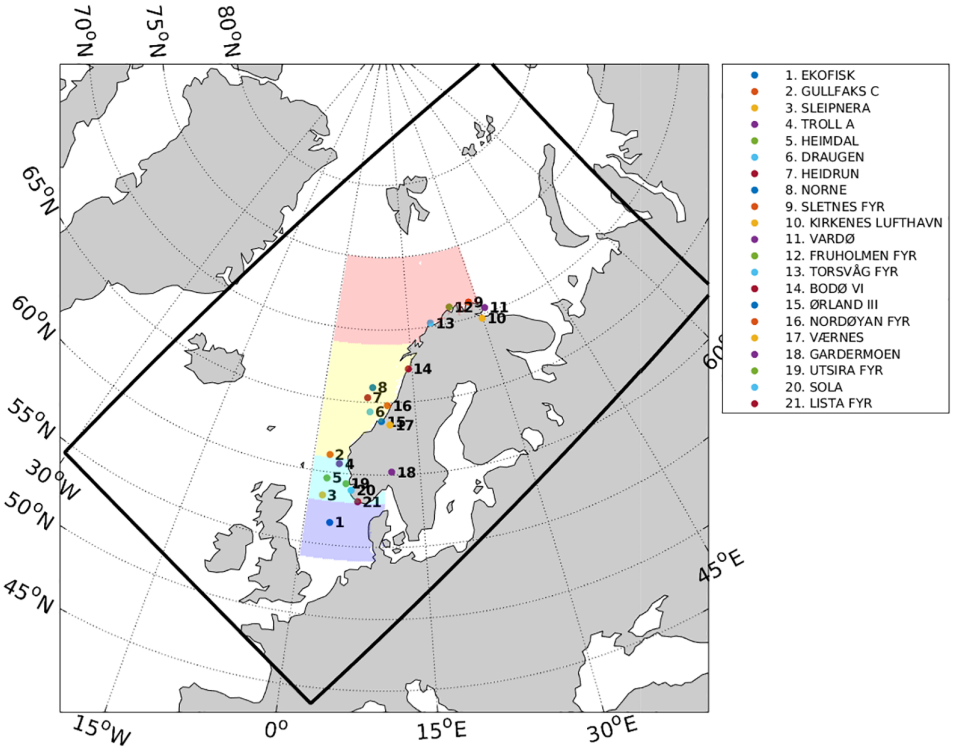

FIGURE 1 Overview of the model domain with offshore and coastal stations. The domains used for trend analysis are coloured. The domains are numbered 1–4 from south to north [Colour figure can be viewed at wileyonlinelibrary.com]

The model grid orientation and resolution are identical to the atmospheric grid. The two-dimensional spectrum is discretized with 24 directional bins (15° resolution) and 25 logarithmically spaced frequency bins, ranging from 0.042 to 0.41 Hz in 10% increments.

3 | GENERAL PERFORMANCE OF NORA10EI

NORA10EI is compared against NORA10, the combined ERA-40 reanalysis/ECMWF analysis (hereafter referred to as EC), ERA-Interim and the more recent reanalysis ERA-5. Norwegian observations, retrieved from the climate database operated by the Norwegian Meteorological Institute, form the basis for the validation.[1] The observation locations are indicated in Figure 1, where the stations 1–8 are offshore and stations 9–21 are onshore. The offshore stations provide discontinuous measurements over the period investigated, 1979–2017, and will not be used in the performance appraisal. All the onshore stations have reliable and relatively continuous measurement series over this period where the requirement has been at least 60% coverage every month. Observations have been despiked by removing observations deviating by more than 20 $m \cdot s^{-1}$ from the hindcasts or the reanalyses. All onshore stations are used in the assessment of the general performance of NORA10EI together with the two arctic stations, Jan Mayen and Hopen, which also meet the requirements.

The validation is based on a total of 753,403 wind measurements. Figure 2 compares the Weibull distribution (Zong, 2006) of these wind measurements against the Weibull distribution of the two hindcasts, NORA10EI, NORA10, and the three reanalyses, EC, ERA-Interim and ERA-5. All three reanalyses exhibit significant overestimation of the frequency of wind speed in the interval 3–10 $m \cdot s^{-1}$ and an underestimation of wind speed above 11 $m \cdot s^{-1}$. The two hindcasts show the same pattern, but with less deviation from the observations. Most significant improvements from the reanalyses are seen for wind speeds between 4 and 5 $m \cdot s^{-1}$ and for wind speeds higher than 11 $m \cdot s^{-1}$.

Figure 3 shows the general performance of the two hindcasts, NORA10EI and NORA10 together with the reanalyses EC, ERA-Interim and ERA-5, expressed by mean error (bias), root mean square error (RMSE) and the correlation with observations (panels a, b, and c, respectively).

The time series of the mean error (Figure 3a) shows that both the hindcasts and the host reanalyses primarily underestimate the wind speed, except for EC in the period 2006–2011. The hindcasts show shorter periods

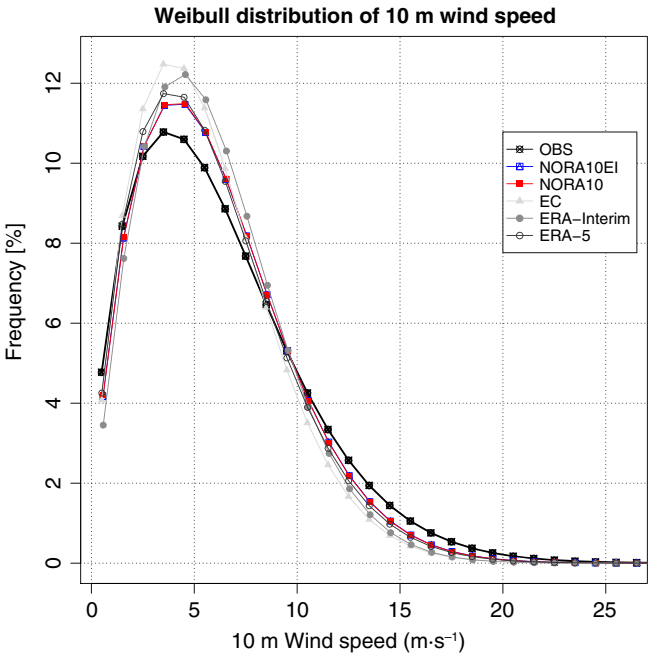

FIGURE 2 Weibull distribution plot of 10 m wind speed for onshore measuring stations [Colour figure can be viewed at wileyonlinelibrary.com]

with weak positive mean errors, however, the negative mean errors dominate the time series. The underestimation in wind speed is considerably smaller for NORA10EI and NORA10 than for EC and ERA-5, but very close to ERA-Interim up to 2002. From 2007 and forwards, NORA10 is the best performing of the hindcasts and the reanalyses, if we ignore the EC for the years 2012 and 2013. The performances of NORA10 and NORA10EI are also more stable, with smaller changes in mean error from year to year compared with the reanalyses. (The range interval in mean error is less than 0.4 $m \cdot s^{-1}$ for the hindcasts, equal to 0.4 $m \cdot s^{-1}$ for ERA-5, 0.5 $m \cdot s^{-1}$ for ERA-Interim and 1.2 $m \cdot s^{-1}$ for the EC.)

Before 2002, the underestimation is greatest in EC and smallest in NORA10EI. The transition from ERA-40 to ECMWF analysis in 2002 is clearly visible by the abrupt change from a strong underestimation of the wind speed before 2002 to a weak overestimation in the years 2006–2011.

This change in mean error in the EC time series has only a small impact on the NORA10 mean error, but the impact of changing the forcing of NORA10 is sufficient to cause a shift in the performance level. While NORA10EI outperforms NORA10 before 2002, NORA10 marginally outperforms NORA10EI in the second period of NORA10 (the mean error is reported for the period 2002–2017 in Table 1).

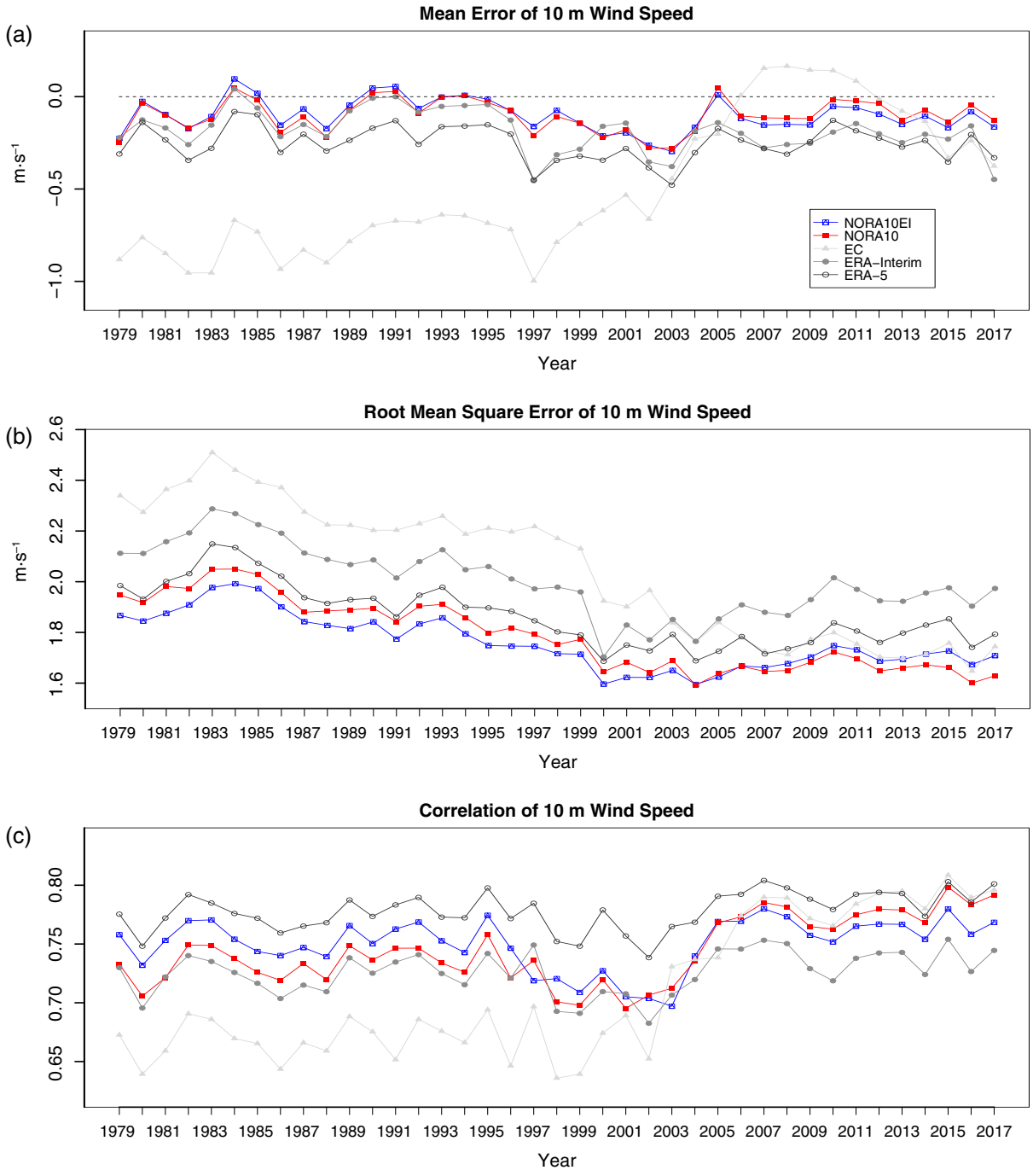

FIGURE 3 General model wind speed performance expressed by mean error (a), root mean square error (b) and the correlation to the observations (c). EC (light grey) represents ERA-40 up to September 2002 and ECMWF analyses thereafter [Colour figure can be viewed at wileyonlinelibrary.com]

The RMSE time series (Figure 3b) shows that NORA10EI has the lowest RMSE in the period 1979–2002. The RMSE is almost the same for the two hindcast in the period 2004 to 2006, while NORA10 outperforms NORA10EI after 2006.

The decrease in RMSE over time for the host analyses (EC analysis and ERA-Interim, respectively) is almost uniformly in the period up to 2000, ignoring the first 5 years. This trend is also found in the hindcasts and in ERA-5, however, the decrease is considerably weaker. From 2003 to 2005, the RMSE of ERA-Interim and the EC operational analyses are almost identical, while the EC operational analysis outperforms ERA-Interim from 2006 (the RMSE is reported for the period 2002–2017 in Table 2).

The time series of the correlation between the hindcasts and the observations and between the

TABLE 1 Mean error from 2002 to 2017 for the models NORA10EI, NORA10, ERA-40/EC, ERA-interim and ERA-5

Year	NORA10EI	NORA10	ERA-40/EC	ERA-interim	ERA-5
2002	−0.26	−0.28	−0.66	−0.35	−0.39
2003	−0.30	−0.28	−0.45	−0.38	−0.48
2004	−0.17	−0.19	−0.23	−0.19	−0.30
2005	0.01	0.05	−0.20	−0.14	−0.17
2006	−0.12	−0.10	0.01	−0.20	−0.24
2007	−0.15	−0.12	0.15	−0.28	−0.28
2008	−0.15	−0.12	0.17	−0.26	−0.31
2009	−0.15	−0.12	0.14	−0.25	−0.24
2010	−0.05	−0.02	0.14	−0.19	−0.13
2011	−0.06	−0.02	0.08	−0.15	−0.18
2012	−0.09	−0.04	−0.01	−0.20	−0.22
2013	−0.15	−0.13	−0.08	−0.25	−0.27
2014	−0.11	−0.07	−0.13	−0.20	−0.24
2015	−0.17	−0.14	−0.33	−0.23	−0.35
2016	−0.08	−0.05	−0.24	−0.16	−0.21
2017	−0.16	−0.13	−0.38	−0.45	−0.33

TABLE 2 Root mean square error from 2002 to 2017 for the models NORA10EI, NORA10, ERA-40/EC, ERA-interim and ERA-5

Year	NORA10EI	NORA10	ERA-40/EC	ERA-interim	ERA-5
2002	1.62	1.64	1.97	1.77	1.73
2003	1.65	1.69	1.84	1.85	1.79
2004	1.60	1.59	1.76	1.77	1.69
2005	1.62	1.64	1.84	1.85	1.73
2006	1.67	1.67	1.78	1.91	1.78
2007	1.66	1.65	1.73	1.88	1.72
2008	1.68	1.65	1.71	1.87	1.74
2009	1.70	1.68	1.77	1.93	1.76
2010	1.75	1.72	1.80	2.02	1.84
2011	1.73	1.70	1.75	1.97	1.81
2012	1.69	1.65	1.70	1.93	1.76
2013	1.69	1.66	1.70	1.92	1.80
2014	1.72	1.67	1.71	1.96	1.83
2015	1.73	1.66	1.76	1.98	1.85
2016	1.67	1.60	1.65	1.90	1.74
2017	1.71	1.63	1.74	1.97	1.79

reanalyses and the observations (Figure 3c) show that ERA-5 yields the highest correlation overall. However, ERA-5 is biased low in wind speed. NORA10EI is as expected surpassed by NORA10 in the last part of the period. EC outperforms ERA-Interim from 2006, as must be expected as it is built on the operational model version of the ECMWF Integrated Forecast System (IFS) that became operational in December 2006 (Cy31r2). Note, however, that EC analysis is very close in performance to ERA-Interim even in the period 2003–2006, as its resolution is about 40 km in 2002 and thus much higher than the resolution of ERA-Interim (79 km).

Figure 3 and Tables 1–3 demonstrate the effect of increased resolution and improved model physics in the host analysis. In September 2002, the resolution of the host analysis to NORA10 was changed from approximately 125 km to about 40 km with the transition from ERA-40 to operational ECMWF analyses. The transition

TABLE 3 Correlation coefficient from 2002 to 2017 for the models NORA10EI, NORA10, ERA-40/EC, ERA-interim and ERA-5

Year	NORA10EI	NORA10	ERA-40/EC	ERA-interim	ERA-5
2002	0.70	0.71	0.65	0.68	0.74
2003	0.70	0.71	0.73	0.71	0.77
2004	0.74	0.74	0.74	0.72	0.77
2005	0.77	0.77	0.74	0.75	0.79
2006	0.77	0.77	0.77	0.75	0.79
2007	0.78	0.79	0.79	0.75	0.80
2008	0.77	0.78	0.79	0.75	0.80
2009	0.76	0.77	0.77	0.73	0.79
2010	0.75	0.76	0.77	0.72	0.78
2011	0.77	0.77	0.78	0.74	0.79
2012	0.77	0.78	0.79	0.74	0.79
2013	0.77	0.78	0.80	0.74	0.79
2014	0.75	0.77	0.78	0.72	0.77
2015	0.78	0.80	0.81	0.75	0.80
2016	0.76	0.78	0.79	0.73	0.79
2017	0.77	0.79	0.80	0.75	0.80

also led to a cycle update from ERA-40's Cy23r4 to the operational Cy25r1.[2] Additional changes to the horizontal resolution of EC occurred in 2006, 2010 and 2016, when the resolution of ECMWF-IFS was refined to 25, 16 and 9 km. Increases in the vertical resolution took place in in 2006 and 2013 to respectively 91 and 137 levels). Four polar low cases have been examined in Appendix A2 (see Figures A1–A8). Although the two hindcasts (NORA10 and NORA10EI) give quite similar results, the lows are somewhat better represented by NORA10EI in the period up to September 2002 (ERA-40 boundary conditions for NORA10), and conversely that NORA10 captures the polar lows better in the period after August 2002.

4 | MEDIAN AND UPPER-PERCENTILE OFFSHORE WIND

Figure 4 shows the 50th (median), 95th and 99th percentiles of observed and modelled 10 m wind speed at offshore stations (stations 1–8 in Figure 1).

The offshore wind stations are very scarce in the early period, with just Ekofisk in operation between period 1980 and 1989. Gullfaks-C started reporting in October 1989, followed by Sleipner and Draugen in 1994 and Heidrun in 1995. Norne and Troll-A started reporting in 1998 and Heimdal in 2005. Offshore stations typically observe winds at heights between 30 and 130 m. The observations are here reduced to 10 m height by using the NORSOK profile defined in Appendix A1.

The median observed wind speed (Figure 4a) ranges from 7.5 to 9.1 $m \cdot s^{-1}$. The first two decades show higher median wind speeds relative to the last part of the period. The median percentile wind speed of NORA10EI ranges from 7.3 to 9.0 $m \cdot s^{-1}$. NORA10EI does also show the highest values in the first 20 years (1979–1998), and somewhat lower values during the last part of the period. This is in agreement with the observations. NORA10 shows slightly higher median wind speeds (ranging from 7.4 to 9.2 $m \cdot s^{-1}$), however, both NORA10EI and NORA10 match the observations well.

EC exhibits a lower range (6.7–8.4 $m \cdot s^{-1}$) for the median wind speed. The trend is also opposite to what is observed with the highest values in the last decade of the period, caused by the change from ERA-40 to operational EC analyses in 2002. ERA-Interim has somewhat higher values than EC (ranging from 6.9 to 8.8 $m \cdot s^{-1}$) and is closer to the observations. The ERA-Interim trends are also similar to the observations, that is, the highest values during the first two decades and somewhat weaker winds during the last part of the period. ERA-5 displays a relatively similar range (7.0–8.6 $m \cdot s^{-1}$).

The 95th percentile observed wind speed varies between 15.2 and 19.8 $m \cdot s^{-1}$. NORA10EI underestimates the 95th percentile (with a range 14.4–17.3 $m \cdot s^{-1}$). The underestimation is quite strong in the beginning of the period but is strongly reduced from 1998, probably caused by increased confidence in the measuring data with the take in of NORNE and TROLL-A. NORA10 exhibits a slightly smaller range in 95th percentiles than NORA10EI,

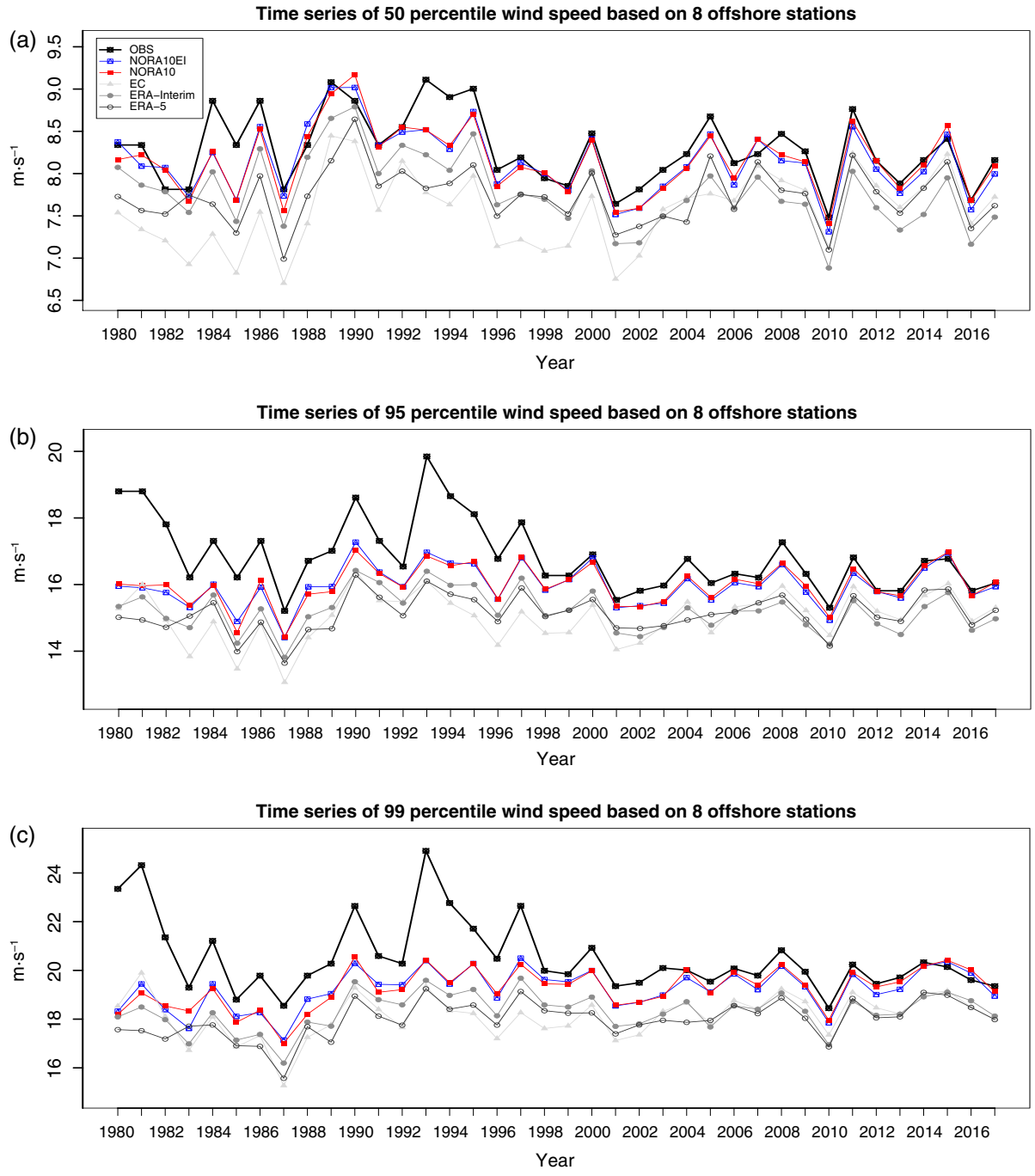

FIGURE 4 Offshore stations, 50th (a), 95th (b) and 99th (c) percentiles of 10-m wind speed ($m \cdot s^{-1}$) [Colour figure can be viewed at wileyonlinelibrary.com]

but the differences are very small. Among the reanalyses, ERA-Interim performs the best in terms of 95th percentile wind speed, closely followed by ERA-5.

The 99th percentile observed wind speed ranges from 18.5 to 24.9 $m \cdot s^{-1}$. NORA10EI and NORA10 both fit the 99th percentile observations in the last part of the period, but underestimate in the first part of the period. The range of NORA10EI is 17.1–20.5 $m \cdot s^{-1}$ and NORA10 displays almost exactly the same range. It is however a question of how credible the observed percentiles in the beginning of the period are, as there are very few observations in the first two decades (see Figure 5).

A general observation from inspection of Figure 3 is that the NORA10 mean error (panel a) and RMSE (panel b) exhibit a weak, decreasing trend, with NORA10 outperforming NORA10EI after 2006. This suggests a small spurious trend in wind speed for NORA10, but, as can be seen from Figure 4, the effect is rather weak.

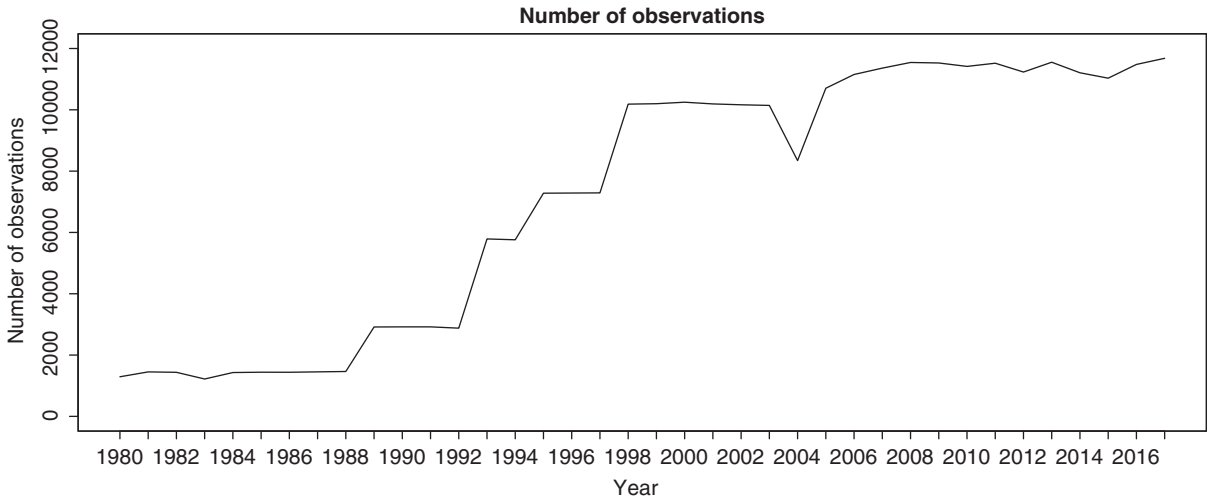

FIGURE 5 Yearly number of observations at offshore stations

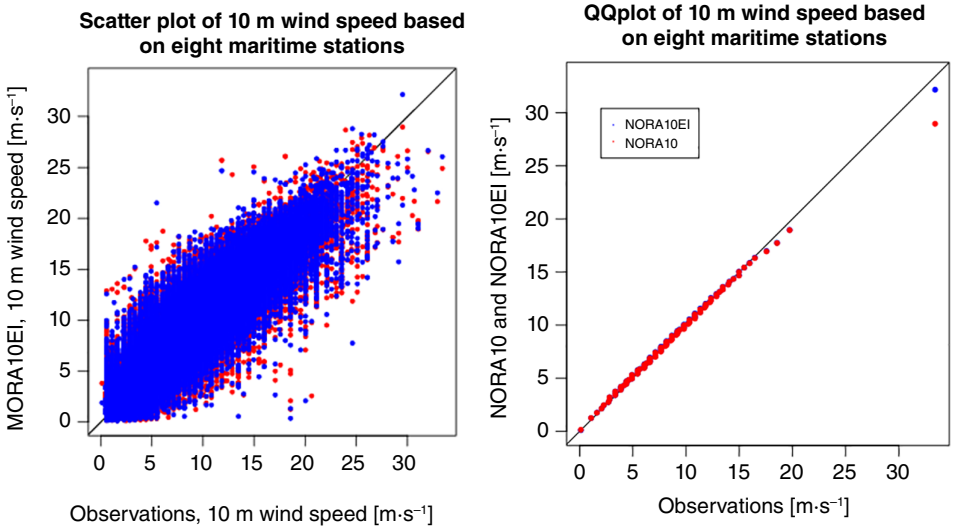

FIGURE 6 Scatter plot (left panel) and quantile-quantile (QQ) plot of 10 m wind speed (right panel) of NORA10EI (blue) and NORA10 (red) against observations from eight offshore stations. The slightly smaller RMSE of NORA10EI is visible in the left panel as smaller spread, but the quantiles (right panel) overlap almost exactly [Colour figure can be viewed at wileyonlinelibrary.com]

Figure 6 shows the quantile-quantile (QQ) comparison of 10-m wind speed and the associated scatter plot based on the eight maritime stations 1–8 in Figure 1. It is clear that the wind speed distributions of NORA10EI and NORA10 are very similar and very close to the observed distribution with NORA10EI showing a slightly better match against the highest observed wind speeds. The slightly lower RMSE of NORA10EI is evident in the slightly smaller spread seen in Figure 6b), but the quantiles very nearly coincide.

5 | OFFSHORE WAVE MEASUREMENTS

The wave model fields have been compared against wave observations of significant wave height, H_s, from a number of offshore platforms in Tables 4 and 5. The performance of NORA10EI is generally slightly better than for NORA10 before 2002, and slightly poorer after 2006, in agreement with the results presented above for the 10-m wind speed. This is illustrated in Figures 7 and 8. The differences are small, and the comparison with observations in generally good. There are no big differences between the two, but NORA10 (red) tends to yield slightly higher H_s after 2006. This tendency is particularly evident in Figure 8 (Draugen field, location 6 in Figure 1), where the 99th percentile (panel b) deviates by as much as 5% toward the end of the period. Ekofisk in the central North Sea (location 1 in Figure 1) exhibits a similar, but weaker, pattern (Figure 7b). The main reason is the small increase in mean wind speed due to higher resolution in EC analyses compared to the early period which is forced with ERA-40, as seen in the trend analysis (Section 6).

TABLE 4 Observed and modelled significant wave height at offshore stations in the Barents Sea and the eastern Norwegian Sea

Location		*N*	Mean	SD	MAD	RMSD	Corr.	P_{90}	P_{95}	P_{99}	$P_{99.9}$
Barents Sea 1978–1998	Obs.	58,637	2.31	1.32				4.1	4.9	6.7	9.2
	NORA10		2.33	1.36	0.34	0.49	0.935	4.2	5.0	6.9	9.3
	NORA10EI		2.35	1.37	0.34	0.47	0.939	4.2	5.0	7.0	9.3
Barents Sea 2007–2015	Obs.	36,003	2.36	1.33				4.1	5.0	6.9	9.1
	NORA10		2.38	1.32	0.32	0.44	0.944	4.2	5.0	6.9	8.9
	NORA10EI		2.33	1.31	0.34	0.47	0.937	4.1	4.9	6.8	8.7
Barents Sea 2007–2015	Obs. 1-hr	108,064	2.36	1.33				4.1	5.0	6.9	9.1
	NORA10EI 1-hr		2.34	1.31	0.34	0.47	0.937	4.1	4.9	6.8	8.8
Haltenbanken 1980–1988	Obs.	12,195	2.68	1.60				4.9	5.9	8.0	10.5
	NORA10		2.57	1.59	0.34	0.47	0.959	4.8	5.8	7.8	10.3
	NORA10EI		2.60	1.61	0.33	0.46	0.960	4.8	5.9	7.9	10.3
Heidrun 1996–2005	Obs.	24,814	2.63	1.50				4.7	5.5	7.4	9.5
	NORA10		2.72	1.61	0.47	0.65	0.917	4.9	5.9	8.1	10.3
	NORA10EI		2.75	1.65	0.48	0.66	0.929	4.9	6.0	8.3	10.7
Heidrun 2006–2017	Obs.	34,170	2.59	1.52				4.7	5.5	7.2	9.8
	NORA10		2.78	1.62	0.45	0.62	0.932	5.0	5.9	8.1	11.1
	NORA10EI		2.75	1.62	0.46	0.63	0.928	4.9	5.9	8.0	11.1
Draugen 1995–2005	Obs.	24,104	2.61	1.65				4.9	5.9	7.8	9.6
	NORA10		2.66	1.61	0.41	0.56	0.941	4.8	5.9	8.1	10.2
	NORA10EI		2.70	1.63	0.42	0.57	0.940	4.9	6.0	8.2	10.7
Draugen 2006–2017	Obs.	30,912	2.69	1.61				4.9	5.9	7.6	9.9
	NORA10		2.81	1.62	0.40	0.54	0.946	5.0	6.0	8.1	10.8
	NORA10EI		2.79	1.62	0.42	0.57	0.941	5.0	6.0	8.0	10.7

TABLE 5 Observed and modelled significant wave height at Norwegian offshore stations in the North Sea

Location		N	Mean	*SD*	MAD	RMSD	Corr.	P_{90}	P_{95}	P_{99}	$P_{99.9}$
Gullfaks 1990–2005	Obs.	38,911	2.69	1.53				4.8	5.7	7.3	9.8
	NORA10		2.76	1.58	0.35	0.49	0.952	4.9	5.9	7.7	10.2
	NORA10EI		2.79	1.60	0.35	0.50	0.953	5.0	6.0	7.8	10.4
Gullfaks 2006–2017	Obs.	30,549	2.79	1.57				4.9	5.8	7.6	9.7
	NORA10		2.84	1.60	0.35	0.47	0.956	5.0	5.9	8.0	10.8
	NORA10EI		2.81	1.59	0.35	0.48	0.954	4.9	5.9	8.0	10.8
Ekofisk 1980–2005	Obs.	67,527	2.07	1.26				3.8	4.5	6.1	8.5
	NORA10		2.07	1.30	0.27	0.41	0.949	3.9	4.6	6.2	8.5
	NORA10EI		2.11	1.32	0.28	0.42	0.948	3.9	4.7	6.3	8.7
Ekofisk 2006–2017	Obs.	29,396	1.98	1.27				3.6	4.4	6.1	8.3
	NORA10		2.09	1.31	0.26	0.37	0.962	3.9	4.7	6.4	9.1
	NORA10EI		2.07	1.31	0.26	0.38	0.958	3.8	4.7	6.4	9.1

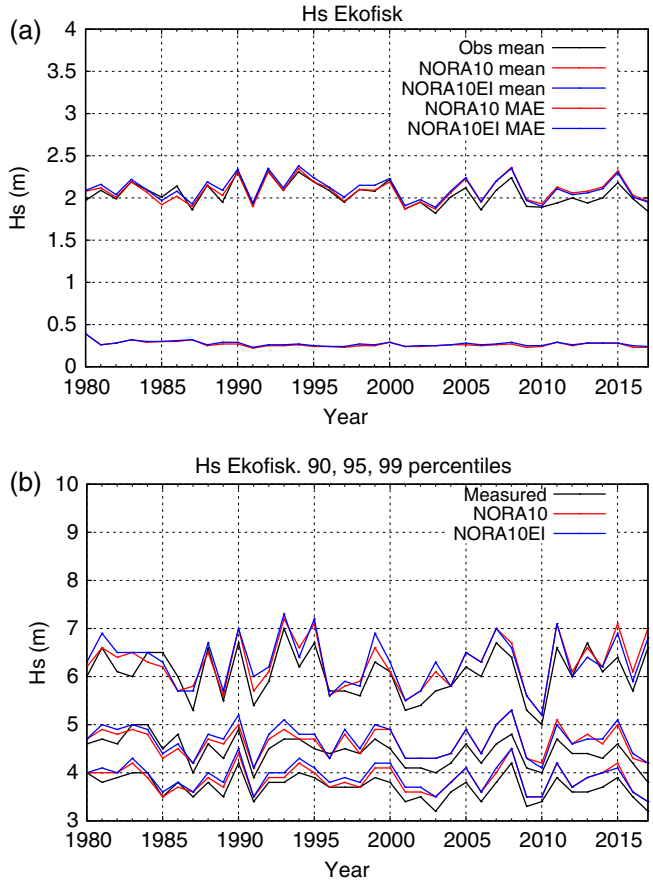

FIGURE 7 (a) Time series of the annual mean significant wave height and the mean absolute error at Ekofisk in the Central North Sea (location 1 in Figure 1). (b) Time series of the 90th, 95th and 99th percentiles of significant wave height [Colour figure can be viewed at wileyonlinelibrary.com]

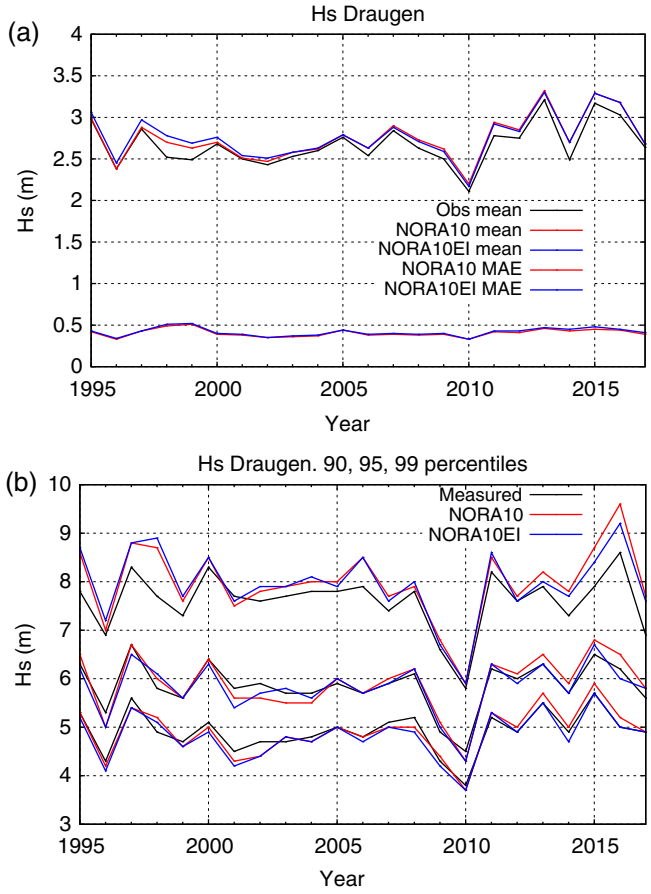

FIGURE 8 (a) Time series of the annual mean significant wave height and the mean absolute error at Draugen in the eastern Norwegian Sea (location 6 in Figure 1). (b) Time series of the 90th, 95th and 99th percentiles of significant wave height [Colour figure can be viewed at wileyonlinelibrary.com]

6 | TRENDS IN MARINE WIND CLIMATE

It is generally difficult to estimate trends from reanalyses as updates to the observation network can lead to spurious trends, even with no changes to the model setup or to the assimilation scheme. ERA-Interim is no exception, as Aarnes *et al*. (2015) demonstrated. It is however clear that the trends found in the downscaled hindcast are somewhat more robust than those of the reanalysis itself. This is because the impact of the assimilation scheme is significantly weakened when the reanalysis is employed as a host analysis providing boundary and initial conditions for short-range forecasts with no assimilation. We do not see strong evidence of spurious trends throughout the model period, but the mean error is slightly more stationary for NORA10EI than for NORA10 (see upper panel, Figure 3, where the wind speed bias for all quality-controlled stations is shown). The RMSE (panel b) is also more stationary for NORA10EI than NORA10, and the correlation (panel c) is significantly higher near the beginning of the period for NORA10EI compared to NORA10. These differences are however small and in the open ocean even smaller (see Figure 4).

Figure 9 shows the median and the 95th and 99th percentiles 10-m wind speed from NORA10EI at four offshore domains (shown in Figure 1) with trends calculated using Sen's slope (see Appendix A3).

Figure 9 shows that Domain 1 has typically the highest median wind speed, but among the lowest 99th percentile wind speeds. Domain 4 has typically the lowest values of both median and upper percentiles. Domain 2 has the strongest wind speeds with 19.6 $m \cdot s^{-1}$ in mean of the 99th percentile wind speed compared to 19.3 $m \cdot s^{-1}$ for Domain 3.

The trend of the median and the 95th percentile wind speed is negative for all domains (see Table 6, NORA10EI). The values range between −0.008 (Domain 3) to −0.067 $m \cdot s^{-1}$ $decade^{-1}$ (Domain 2) for the 50th percentile and − 0.029 (Domain 1) to −0.087 $m \cdot s^{-1}$ $decade^{-1}$ (Domain 4) for the 95th percentile.

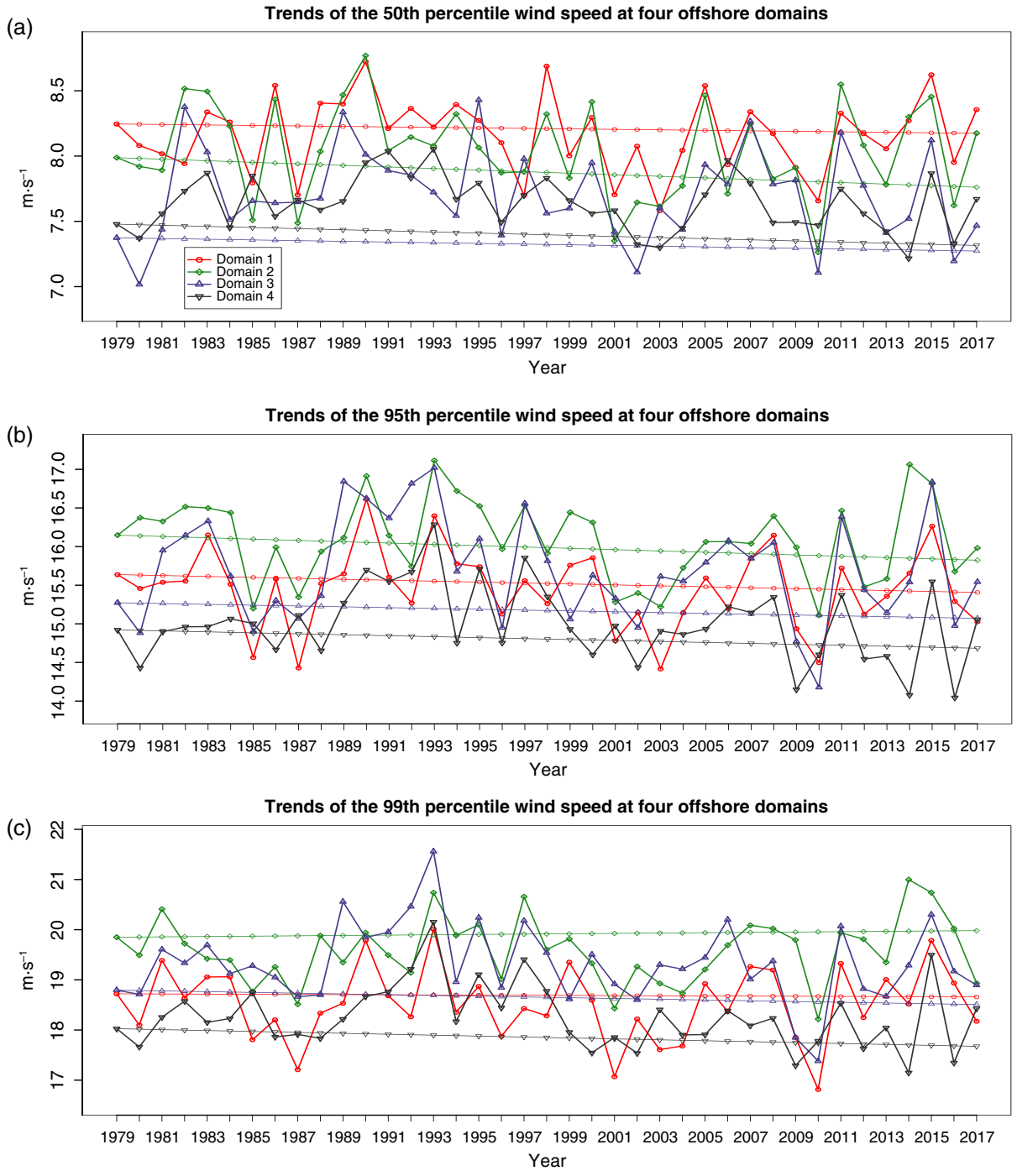

FIGURE 9 NORA10EI time series of the trend in 50th (a), 95th (b) and 99th (c) percentile 10 m wind speed at the four different offshore domains shown in Figure 1 [Colour figure can be viewed at wileyonlinelibrary.com]

The 99th percentile shows a decreasing trend for Domains 3 and 4 and an increasing trend for Domains 1 and 2. The signs of the trends are also in agreement with Figures 10b and 11b, which are discussed in Section 7. The decreasing trends of the 99th percentile are -0.067 m·s^{-1} decade^{-1} for Domain 3 and -0.128 m·s^{-1} decade^{-1} for Domain 4. The increasing trends of the 99th percentile are $+0.020$ m·s^{-1} decade^{-1} for Domain 1 and $+0.075$ m·s^{-1} decade^{-1} for Domain 2. Both the decreasing trends and the increasing trends are small and none of the NORA10EI trends are statistically significant at 95% confidence level.

Table 6 summarizes the trends for NORA10, ERA-Interim and ERA-40/EC. While a weak negative trend dominates in NORA10EI, NORA10 shows a balance between weak positive and weak negative trends.

TABLE 6 A 10-m wind speed trend estimates based on Sen's slope and the statistically significant threshold

Domain	Trend in 50th percentile wind speed ($m\ s^{-1}$ $decade^{-1}$) With significance threshold (%)	Trend in 95th percentile wind speed ($m\ s^{-1}$ $decade^{-1}$) With significance threshold (%)	Trend in 99th percentile wind speed ($m\ s^{-1}$ $decade^{-1}$) With significance threshold (%)
NORA10EI			
Domain 1	−0.032 *43.6*	−0.029 *70.6*	+0.020 *88.0*
Domain 2	−0.067 *25.8*	−0.101 *29.1*	+0.075 *49.7*
Domain 3	−0.008 *92.0*	−0.058 *61.5*	−0.067 *54.6*
Domain 4	−0.044 *18.3*	−0.087 *32.7*	−0.128 *15.9*
NORA10			
Domain 1	+0.029 *43.9*	−0.015 *84.7*	+0.076 *49.8*
Domain 2	−0.004 *96.1*	+0.112 *24.6*	−0.008 *92.3*
Domain 3	+0.018 *71.7*	−0.017 *92.3*	+0.026 *82.8*
Domain 4	+0.019 *54.5*	−0.035 *54.5*	+0.051 *59.5*
ERA-interim			
Domain 1	−0.018 *54.5*	−0.123 *14.0*	−0.059 *59.5*
Domain 2	−0.068 *17.5*	−0.132 *8.2*	−0.101 *27.6*
Domain 3	−0.044 *56.1*	−0.077 *45.3*	−0.095 *32.1*
Domain 4	−0.043 *18.3*	−0.055 *38.4*	−0.094 *29.8*
ERA40/EC			
Domain 1	+0.270 *0.0*	+0.033 *62.8*	−0.044 *73.5*
Domain 2	+0.354 *0.0*	+0.331 *0.0*	+0.395 *0.0*
Domain 3	+0.343 *0.0*	+0.401 *0.0*	+0.380 *0.5*
Domain 4	+0.256 *0.0*	+0.302 *0.0*	+0.299 *0.0*

Note: Note that the combined trend estimates for ERA-40 and ECMWF analyses are included here for reference as they represent that boundary forcing for NORA10. Significance threshold values are given as italic.

Unsurprisingly, the transition from ERA-40 to EC analyses shows a relatively strong positive trend for all the domains and for all the three percentiles investigated, except for the 99th percentile trend for Domain 1. Finally, ERA-Interim shows uniformly negative trends.

The slightly stronger positive trends (and weaker negative trends) in NORA10 compared to NORA10EI are mainly caused by the change in boundary conditions from ERA-40 to ECMWF operational analyses in September 2002. Note that these trends are all weak and in fact not statistically significant. Interestingly, the relatively minor differences seen between NORA10 and NORA10EI demonstrate that the hindcasts are quite insensitive to resolution changes in the host analysis. This is also in accordance with Davis (2014) who showed that little error can be clearly ascribed to the lateral boundary conditions with a proper choice of domain.

7 | SPATIAL WIND PATTERNS

Figure 10 shows the mean wind speed in the two periods related to the two different forcing periods of NORA10, 1979–2002 and 2002–2017. The general picture shows decreasing wind speed from west to east between Iceland and Great Britain, and from north to south in the North sea and from south to north in the Norwegian Sea and the Greenland Sea. This pattern reflects the synoptic-scale picture with frequent low-pressure systems moving eastward over the Atlantic and weakening as the systems approach land and when they travel northward into the Barents Sea. This pattern is clearly visible in both periods. The mean wind speed ranges from 4 to 10 $m{\cdot}s^{-1}$ over the ocean. Figure 10b) shows the difference between the two periods for NORA10EI and for NORA10. Except for the Arctic region, NORA10EI exhibits only minor differences between the two periods. NORA10 shows weakly

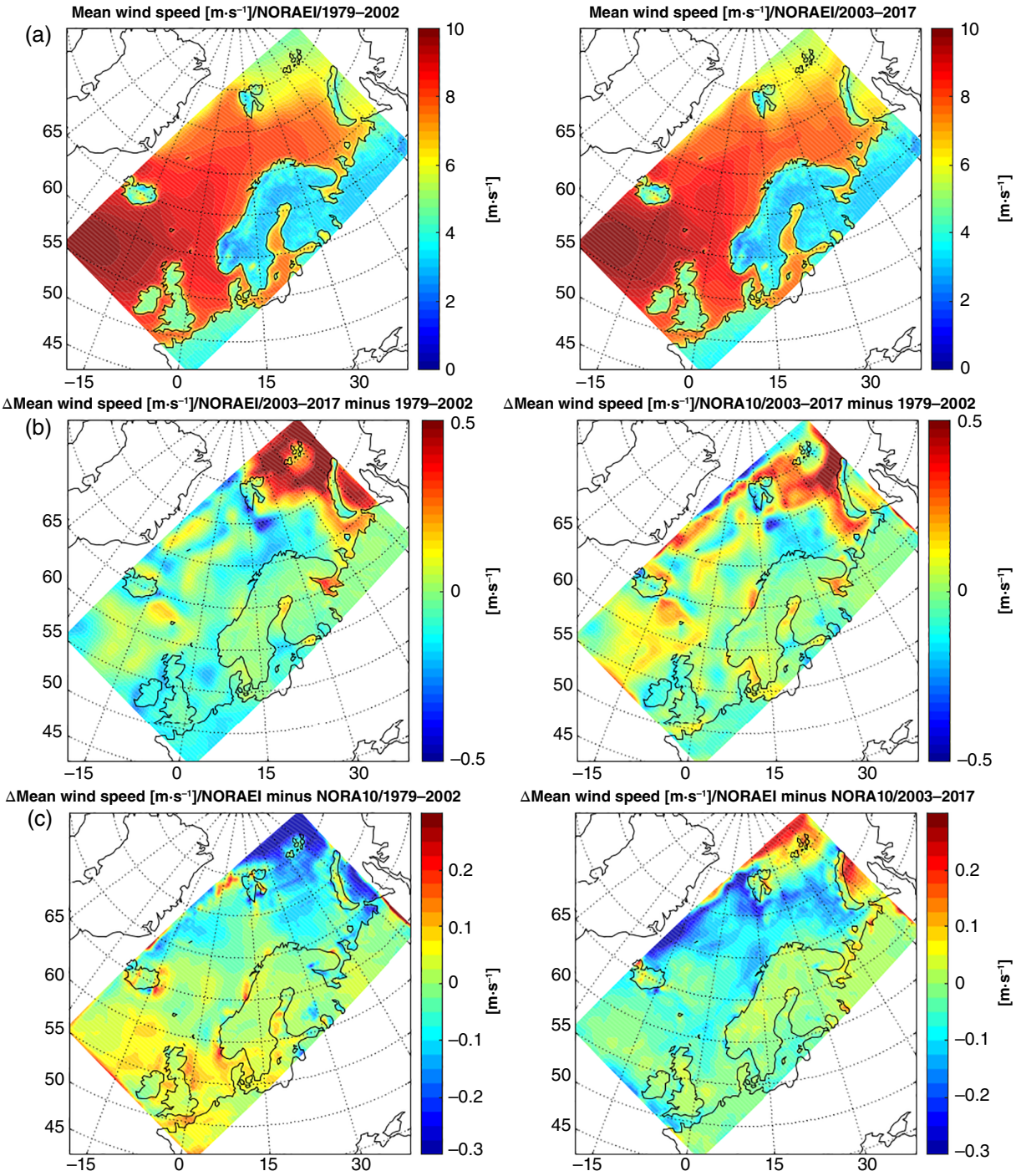

FIGURE 10 Map of mean wind speed in (a) NORA10EI (left) in the first (1979–2002) and (right) second period (2003–2017), (b) the difference between the second and first period in NORA10EI (left) and NORA10 (right), and (c) the difference between NORA10EI (left) and NORA10 (right) in the first and the second period [Colour figure can be viewed at wileyonlinelibrary.com]

increasing wind speed in large parts of the domain. Common to the two hindcasts is an increase in wind speed south and south-east of Iceland, and in the Greenland Sea. The difference in wind speed between the two periods also agrees quite well with the trend analysis performed in Section 6. Because of the lack of reliable long-term measurements for the Arctic, we will not focus on the Arctic area here. However, due to receding sea ice cover, we expect considerable changes in wind speed and waves in this area (Aarnes *et al.*, 2017; Waseda *et al.*, 2018; Morim *et al.*, 2019). Figure 10c) shows the difference between NORA10EI and NORA10 in the first and the second period. In the first period, the wind speed is stronger in NORA10EI in the southern part of the

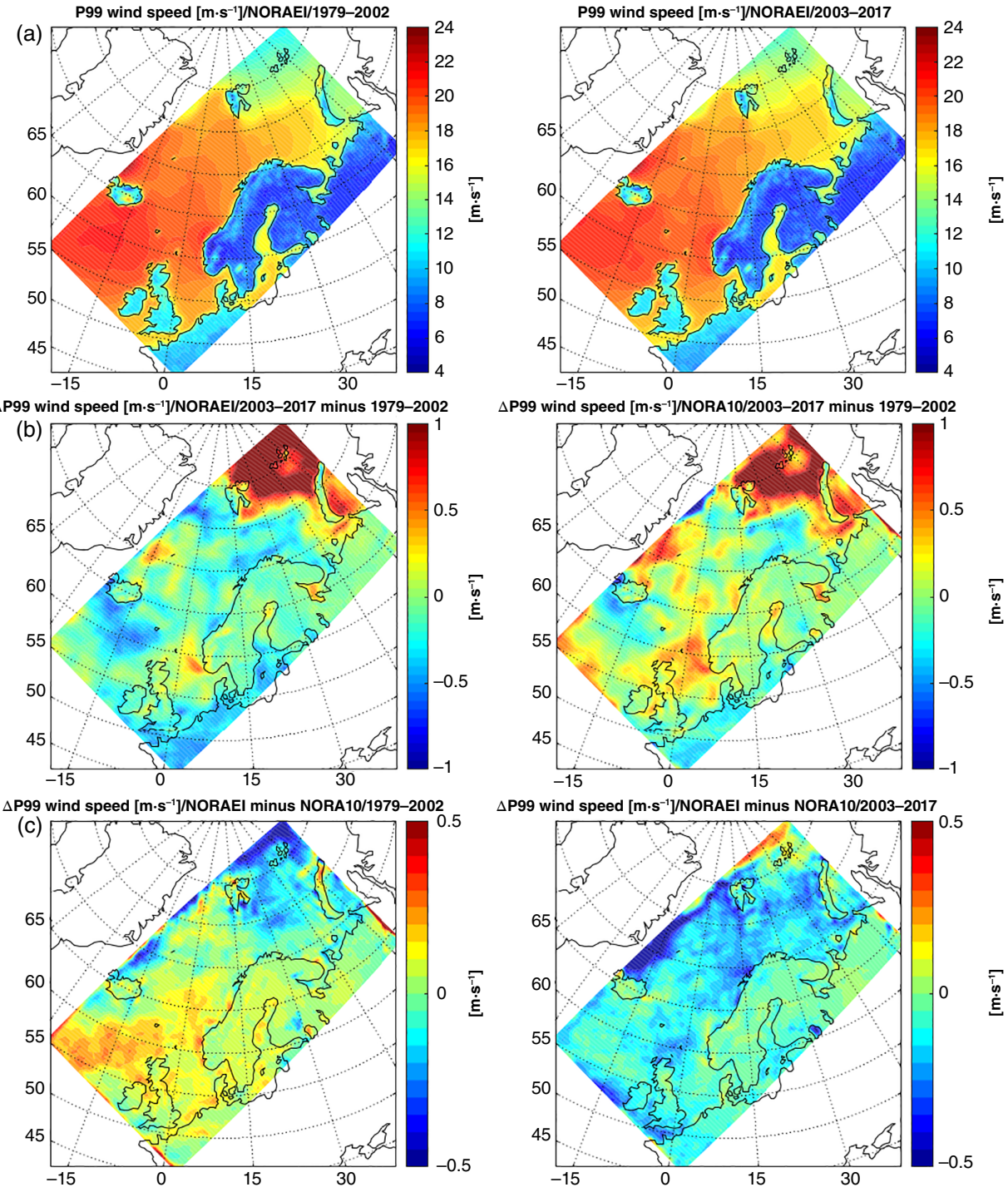

FIGURE 11 Map of the 99th percentile wind speed (a) NORA10EI (left) in the first (1979–2002) and (right) second period (2003–2017), (b) the difference between the second and first period in NORA10EI (left) and NORA10 (right), and (c) the difference between NORA10EI (left) and NORA10 (right) in the first and the second period [Colour figure can be viewed at wileyonlinelibrary.com]

domain, and weaker in the northern part of the domain. In the second period, the two models are more equal and the differences are mostly limited to different inflow at the boundaries. NORA10 shows stronger inflow between 65° and 80°N, but NORA10EI still has stronger wind speed over the sea ice north of 80°N.

Figure 11 shows the 99th percentile wind speed. It is clear that the upper percentiles exhibit the same spatial pattern as the mean values in Figure 10, but with values ranging from 13 to above 20 $m \cdot s^{-1}$ over the ocean. Figure 11b) shows the difference between the two periods for NORA10EI and for NORA10.

While NORA10 showed an increase in mean wind speed over large parts of the ocean, which was not visible in NORA10EI, NORA10EI shows an increase up to 0.5 $m \cdot s^{-1}$ offshore from western Norway. NORA10EI also shows an increase in wind speed over the northern part of Great Britain and a strong increase north of Svalbard. NORA10 shows the same pattern, however, with even stronger increase in wind speed in the southern part of the domain. Figure 11c) shows the difference between the 99th percentile of NORA10EI and NORA10 in the first and the second period. NORA10EI has higher 99th percentile wind speeds in the southern domain in the first period and weaker wind speeds than NORA10 in the second period, as can be expected based on the differences between their host analyses.

8 | EXTREME VALUE ESTIMATES OF WIND SPEED AND SIGNIFICANT WAVE HEIGHT

The comparison of trends in mean and upper percentile wind speed and significant wave height suggest that the differences are small, and that the impact of the transition in boundary forcing used in NORA10 has had negligible impact on the overall statistics. As a further test of this, we compare the return value estimates from annual maxima of wind speed and significant wave height in NORA10 and NORA10EI.

The procedure follows that outlined by Aarnes *et al.* (2012) where a generalized extreme value (GEV) distribution is fitted to annual (block) maxima (see Coles, 2001, pp 45–51). The GEV distribution is an asymptotic limit

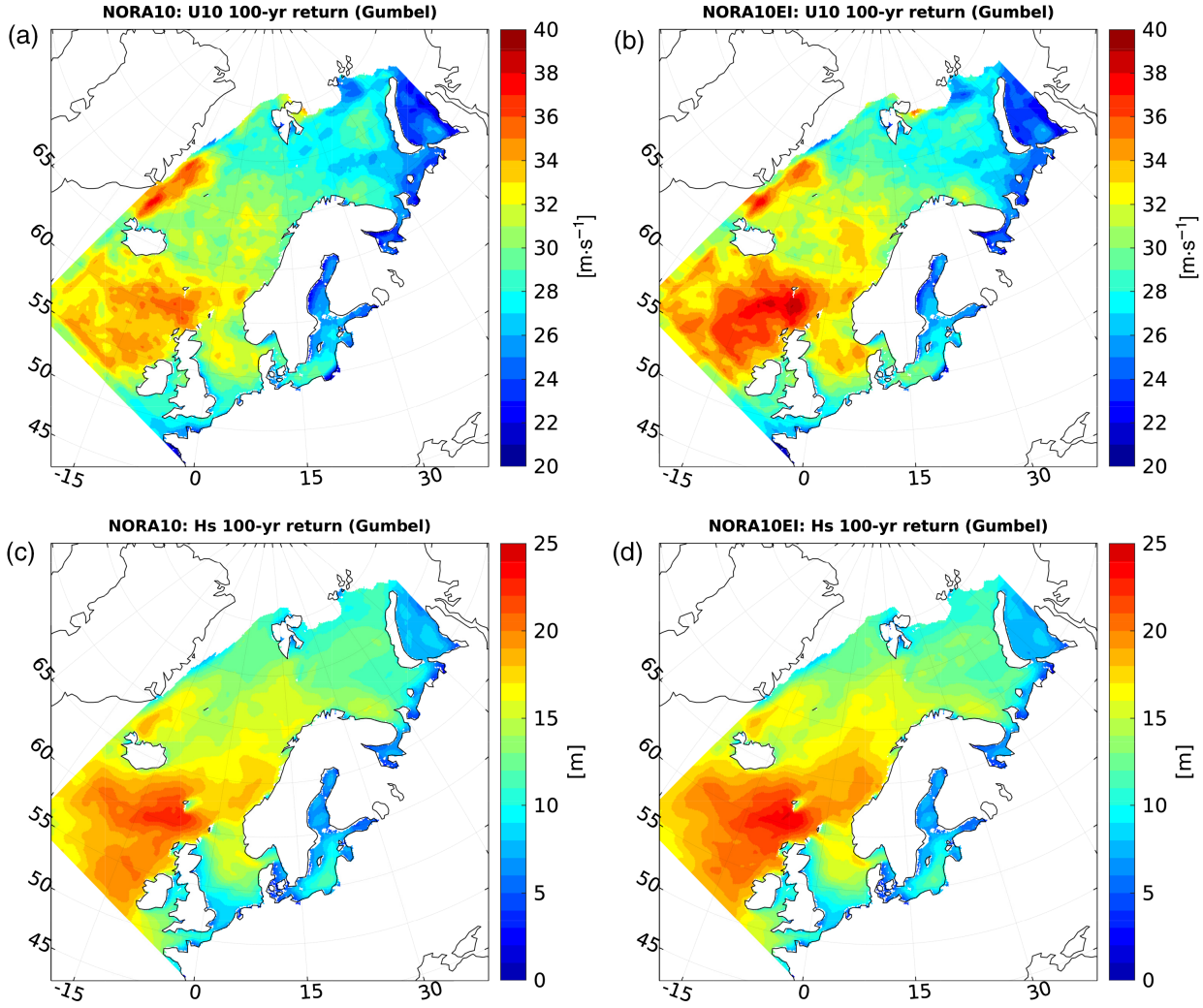

FIGURE 12 Map of 100 year return values of 10 m wind speed (upper panels) and significant wave height (lower panels). The NORA10 return value estimates are shown on the left (a) and (c) for the period 1979–2017. The corresponding estimates for NORA10EI are found on the right (b) and (d). The NORA10EI estimates are higher than the NORA10 estimates, particularly in wind speed (up to 5 $m \cdot s^{-1}$ difference), and considerably less in significant wave height [Colour figure can be viewed at wileyonlinelibrary.com]

for a distribution of blocked maxima $M_n = \max\{X_1, X_2, ..., X_n\}$. Following Coles (2001), the cumulative distribution function (CDF) of the block maxima formed from a random sequence of independent variables can be written

$$G(z) = \exp\left\{ -\left[1+\xi\left(\frac{z-\mu_n}{\sigma_n}\right)\right]^{-1/\xi}\right\}, \quad (1)$$

where σ_n is the scale parameter, μ_n is known as the location parameter, and ξ is the so-called shape parameter. The GEV distribution contains as special cases the Fréchet ($\xi > 0$), Gumbel ($\xi = 0$) and reversed Weibull ($\xi < 0$) distributions. In the following analysis, we use the Gumbel distribution, fitted using a maximum likelihood method (Coles, 2001). This has the desired effect of creating smoother spatial return value estimates than the full GEV, making it easier to compare the two datasets.

Figure 12 contrasts the 100-year return value estimates for U_{10} and H_s. For consistency, the NORA10 estimates (a) and (c) are based on the same period as NORA10EI (b) and (d), that is, 1979–2017. It is clear that NORA10EI yield somewhat higher return values than NORA10, both for U_{10} and H_s, especially in the region south of Iceland and north-west of Scotland. Here, the 100-year return value for wind speed increase from 35 to 40 $m \cdot s^{-1}$ between the Faroe islands and Scotland. This gives a slight increase in 100-year return estimates of the significant wave height from 22 to 24 m in the same region. Although these changes are not dramatic, it shows that using EC analysis to force NORA10 has not led to particularly high return estimates, rather the opposite. It is however important to note that the return values are based on just 29 years, which is considered a short period for extreme value analysis, and represents a much smaller data set than other recent extreme value estimates of wind speed and significant wave height (Breivik *et al.*, 2013, 2014; Meucci *et al.*, 2018). This means that the impact of individual storms becomes large (Aarnes *et al.*, 2012).

9 | DISCUSSION

This study was motivated by the question of non-stationarity in NORA10 at the changeover from using ERA-40 to using ECMWF analyses as initial and boundary conditions. The results show that the stationarity issue is of negligible importance, although we do see a decreasing bias and RMSE and increasing correlation with wind observations in the second part of NORA10 (Figure 3).

The maps in Figure 10 reveal a larger negative wind speed bias in NORA10 compared with NORA10EI in the first period (1979–2002) in the North Sea and the Norwegian Sea, but a better match in the second period (2003–2017). This explains the weak positive trends in NORA10 which are not reproduced by NORA10EI. However, over most parts of the oceans, the two hindcasts show a large degree of similarity despite differences in boundary and initial conditions. Since the two hindcasts employ the same numerical weather prediction model at the identical horizontal and vertical resolutions, the only differences stem from the boundary and surface forcing.

The weak trends in wind speed in NORA10EI are in agreement with other studies for northwestern Europe and the North-eastern Atlantic (Ciavola *et al.*, 2011; Cusack, 2013; Feser *et al.*, 2015; Minola *et al.*, 2016).

10 | CONCLUSIONS AND FURTHER WORK

The NORA10EI hindcast is generally found to be in close agreement with NORA10. This study, and the generation of the NORA10EI hindcast, was in part motivated by a need to test the impact of an abrupt change in the forcing fields in the NORA10 hindcast as it is extensively used for extreme value analysis and climatological studies of wind and wave height in the North Sea, the Norwegian Sea and the Barents Sea (Aarnes *et al.*, 2012; Furevik and Haakenstad, 2012; Bruserud and Haver, 2016), but more generally to look for the impact of host analysis on regional hindcasts. We find a slight reduction in the mean wind speed trend compared with NORA10, and as expected the bias and RMSE are more stationary. This does not appear to have a major impact on the upper percentiles, although, and the two hindcasts are in close agreement with each other for the offshore locations analysed. The representation of polar lows was qualitatively found to be slightly better in NORA10EI in the period before September 2002 (the host reanalysis ERA-Interim is superior to ERA-40). The difference is again small, and it is clear that a better host model and higher resolution of the hindcast itself is required before a proper representation of polar lows can be expected. Improved reanalyses are now available, in particular the new ERA-5 (Hersbach and Dee, 2016), and work is now underway to assess the required resolution for the next generation hindcast archive. The AROME atmospheric model (Seity *et al.*, 2011) is one candidate to be tested with non-hydrostatic physics and a resolution of the order of 3 km.

ACKNOWLEDGMENTS

This study was carried out with support from the ERA4CS WINDSURFER project and the Norwegian Climate Service Centre (KSS). The hindcast archive was

made possible with computational resources provided by NOTUR, http://www.sigma2.no, on the Vilje national supercomputing facility. The Norwegian Deepwater Programme and later Equinor ASA funded the development of the NORA10 archive. MR, OJA and ØB acknowledge the Research Council of Norway for funding through the ExWaMar project (grant no 256466).

ORCID

Øyvind Breivik https://orcid.org/0000-0002-2900-8458

ENDNOTES

[1] https://frost.met.no, last accessed October 2019.

[2] https://www.ecmwf.int/en/forecasts/documentation-and-support/changes-ecmwf-model

[3] https://projects.met.no/stars/

REFERENCES

Aarnes, O.J., Abdalla, S., Bidlot, J.-R. and Breivik, Ø. (2015) Marine wind and wave height trends at different ERA-interim forecast ranges. *Journal of Climate*, 28, 819–837. https://doi.org/10.1175/JCLI-D-14-00470.1.

Aarnes, O.J., Breivik, Ø. and Reistad, M. (2012) Wave extremes in the Northeast Atlantic. *Journal of Climate*, 25, 1529–1543. https://doi.org/10.1175/JCLI-D-11-00132.1.

Aarnes, O.J., et al. (2017) Projected changes in significant wave height towards the end of the 21st century: Northeast Atlantic. *Journal of Geophysical Research, Oceans*, 122, 3394–3403. https://doi.org/10.1002/2016JC012521.

Appendini, C.M., Torres-Freyermuth, A., Salles, P., López-González, J. and Mendoza, E.T. (2014) Wave climate and trends for the gulf of Mexico: a 30-yr wave hindcast. *Journal of Climate*, 27, 1619–1632. https://doi.org/10.1175/JCLI-D-13-00206.1.

Breivik, Ø., Aarnes, O., Abadalla, S., Bidlot, J.-R. and Janssen, P. (2014) Wind and wave extremes over the world oceans from very large ensembles. *Geophysical Research Letters*, 41(14), 5122–5131. https://doi.org/10.1002/2014GL060997.

Breivik, Ø., Aarnes, O.J., Bidlot, J.-R., Carrasco, A. and Saetra, Ø. (2013) Wave extremes in the Northeast Atlantic from ensemble forecasts. *Journal of Climate*, 26, 7525–7540 arXiv:1304.1354, doi:10/mpf.

Breivik, Ø., Gusdal, Y., Furevik, B.R., Aarnes, O.J. and Reistad, M. (2009) Nearshore wave forecasting and hindcasting by dynamical and statistical downscaling. *Journal of Marine Systems*, 78 (2), S235–S243.

Bromirski, P.D., Cayan, D.R., Helly, J. and Wittmann, P. (2013) Wave power variability and trends across the North Pacific. *Journal of Geophysical Research Oceans*, 118(12), 6329–6348. https://doi.org/10.1002/2013JC009189.

Bruserud, K. and Haver, S. (2016) Comparison of wave and current measurements to NORA10 and NoNoCur hindcast data in the northern North Sea. *Ocean Dynamics*, 66(6), 823–838. https://doi.org/10.1007/s10236-016-0953-z.

Buizza, R., Bronnimann, S., Haimberger, L., Laloyaux, P., Martin, M.J., Fuentes, M., et al. (2018) The EU-FP7 ERA-CLIM2 project contribution to advancing science and production of earth system climate reanalyses. *Bulletin of the American Meteorological Society*, 99(5), 1003–1014. https://doi.org/10.1175/BAMS-D-17-0199.1.

Ciavola, P., Ferreira, O., Haerens, P., Koningsveld, M.V., Armaroli, C. and Lequeux, Q. (2011) Storm impacts along European coastlines. Part 1: the joint effort of the MICORE and ConHaz projects. *Environmental Science & Policy*, 14(7), 912–923. https://doi.org/10.1016/j.envsci.2011.05.011.

Coles, S. (2001) *An Introduction to Statistical Modeling of Extreme Values*. Berlin, Germany: Springer Verlag, p. 210.

Compo, G.P., Whitaker, J.S., Sardeshmukh, P.D., Matsui, N., Allan, R.J., Yin, X., et al. (2011) The twentieth century reanalysis project. *Quarterly Journal of the Royal Meteorological Society*, 137(654), 1–28. https://doi.org/10.1002/qj.776.

Cusack, S. (2013) A 101 year record of windstorms in the Netherlands. *Climatic Change*, 116, 693–704. https://doi.org/10.1007/s10584-012-0527-0.

Davis, T. (2014) Lateral boundary conditions for limited area models. *Quarterly Journal of the Royal Meteorological Society*, 140, 185–196.

Dee, D., Uppala, M., Simmons, A.J., Berrisford, P., Poli, P., Kobayashi, S., Andrae, U., et al. (2011) The ERA-interim reanalysis: configuration and performance of the data assimilation system. *Quarterly Journal of the Royal Meteorological Society*, 137(656), 553–597. https://doi.org/10.1002/qj.828.

Douglas, M.W., Shapiro, M.A., Fedor, L.S. and Saukkonen, L. (1995) Research aircraft observations of a polar low at the East Greenland ice edge. *Monthly Weather Review*, 123, 5–15.

Feser, F., Barcikowska, M., Krueger, O., Schenk, F., Weisse, R. and Xia, L. (2015) Storminess over the North Atlantic and northwestern Europe—a review. *Quarterly Journal of the Royal Meteorological Society*, 141, 350–382. https://doi.org/10.1002/qj.2364.

Furevik, B.R. and Haakenstad, H. (2012) Near-surface marine wind profiles from rawinsonde and NORA10 hindcast. *Journal of Geophysical Research*, 117(D23), 14. https://doi.org/10.1029/2012JD018523.

Gaslikova, L. and Weisse, R. (2006) Estimating near-shore wave statistics from regional hindcasts using downscaling techniques. *Ocean Dynamics*, 56(1), 26–35.

Gibson, J., Kallberg, P., Uppala, S., Hernandez-Carrascal, A., Nomura, A., Serrano, E., 1997: ERA Description In ECMWF ERA-15 Project Report Series, No. 1. Tech. rep., European Centre for Medium-Range Weather Forecasting, ECMWF Shinfield, Reading, UK.

Günther, H., Hasselmann, S., and Janssen, P. A. E. M., 1992: Wamodel Cycle 4 (revised version). Tech. Rep. 4, Deutsches KlimaRechenZentrum, Hamburg, Germany.

Haakenstad, H., Reistad, M., Haugen, J., and Breivik, Ø., 2012: Update of the NORA10 hindcast archive for 2011 and a study of polar low cases with the WRF model. Research Report 12/2012, The Norwegian Meteorological Institute, Oslo, Norway, 69 pp.

Hersbach, H. and Dee, D. (2016) ERA5 reanalysis is in production. *ECMWF Newsletter*, 147, 7.

Hersbach, H., Peubey, C., Simmons, A., Berrisford, P., Poli, P. and Dee, D. (2015) ERA-20CM: a twentieth-century atmospheric model ensemble. *Quarterly Journal of the Royal Meteorological Society*, 141(691), 2350–2375. https://doi.org/10.1002/qj.2528.

Hsu, E.A.M., Meindl, E.A. and Gilhousen, D.B. (1994) Determining the power-law wind-profile exponent under near-neutral stability conditions at sea. *Journal of Applied Meteorology*, 33, 757–765.

Izaguirre, C., Méndez, F.J., Espejo, A., Losada, I.J. and Reguero, B. G. (2013) Extreme wave climate changes in Central-South America. *Climatic Change*, 119(2), 277–290. https://doi.org/10.1007/s10584-013-0712-9.

Kalnay, E., Kanamitsu, M., Kistler, R., Collins, W., Deaven, D., Gandin, L., Iredell, M., Saha, S., White, G., Woollen, J., Zhu, Y., Chelliah, M., Ebisuzaki, W., Higgins, W., Janowiak, J., Mo, K.C., Ropelewski, C., Wang, J., Leetmaa, A., Reynolds, R., Jenne, R., and Joseph, D. 1996: The NCEP/NCAR 40-year reanalysis project. *Bulletin of American Meteorological Society*, 77, 437–472, doi:10/fg6rf9.

Kendall, M.G. (1975) *Rank Correlation Methods*. London, UK: Griffin.

Komen, G.J., Cavaleri, L., Donelan, M., Hasselmann, K., Hasselmann, S. and Janssen, P.A.E.M. (1994) *Dynamics and Modelling of Ocean Waves*. Cambridge: Cambridge University Press 532 pp.

Laloyaux, P., and Coauthors, 2018: CERA-20C: a coupled reanalysis of the twentieth century. *Journal of Advances in Modeling Earth Systems*, 10(5), 1172–1195. https://doi.org/10.1029/2018MS001273.

Mann, H. (1945) Nonparametric tests against trend. *Econometrica*, 13, 245–259.

Meucci, A., Young, I.R., Aarnes, O.J. and Breivik, Ø. (2019) Comparison of wind speed and wave height trends from twentieth century models and satellite altimeters. *Journal of Climate*, 33, 611–624. https://doi.org/10.1175/JCLI-D-19-0540.1.

Meucci, A., Young, I.R. and Breivik, Ø. (2018) Wind and wave extremes from atmosphere and wave model ensembles. *Journal of Climate*, 31(21), 8819–8842. https://doi.org/10.1175/JCLI-D-18-0217.1.

Minola, L., Azorin-Molina, C. and Chen, D. (2016) Homogenization and assessment of observed near-surface wind speed trends across Sweden, 1956-2013. *Journal of Climate*, 29, 7397–7415.

Morim, J., et al. (2019) Robustness and uncertainties in global multivariate wind-wave climate projections. *Nature Climate Change*, 9, 711–718. https://doi.org/10.1038/s41558-019-0542-5.

NORSOK, 2007: NORSOK standard: Action and action effects, N-003. Tech. rep., Standard Norge, Postboks 242, 1326 Lysaker.

Onogi, K., et al. (2007) The JRA-25 reanalysis. *Journal of the Meteorological Society of Japan*, 85(3), 369–432. https://doi.org/10.2151/jmsj.85.369.

Poli, P., Hersbach, H., Dee, D.P., Berrisford, P., Simmons, A.J., Vitart, F., Laloyaux, P., Tan, D.G.H., et al. (2016) ERA-20C: an atmospheric reanalysis of the twentieth century. *Journal of Climate*, 29(11), 4083–4097. https://doi.org/10.1175/JCLI-D-15-0556.1.

Rasmussen, E.A. and Turner, J. (2003) *Polar Lows: Mesoscale Weather Systems in the Polar Regions*. Cambridge: Cambridge University Press.

Reistad, M., Breivik, Ø., Haakenstad, H., Aarnes, O.J., Furevik, B.R. and Bidlot, J.-R. (2011) A high-resolution hindcast of wind and waves for the North Sea, the Norwegian Sea, and the Barents Sea. *Journal of Geophysical Research*, 116, 18, C05 019 doi:10/fmnr2m.

Rienecker, M.M., et al. (2011) MERRA: NASA's modern-era retrospective analysis for research and applications. *Journal of Climate*, 24 (14), 3624–3648. https://doi.org/10.1175/JCLI-D-11-00015.1.

Saha, S., et al. (2010) The NCEP climate forecast system reanalysis. *Bulletin of American Meteorological Society*, 91(8), 1015–1057. https://doi.org/10.1175/2010Bams3001.1.

Saha, S., et al. (2014) The NCEP climate forecast system version 2. *Journal of Climate*, 27, 2185–2208. https://doi.org/10.1175/JCLI-D-12-00823.1.

Seity, Y., Brousseau, P., Malardel, S., Hello, G., Benard, P., Bouttier, F., Lac, C. and Masson, V. (2011) The AROME-France convective-scale operational model. *Monthly Weather Review*, 139(3), 976–991. https://doi.org/10.1175/2010MWR3425.1.

Semedo, A., Sušelj, K., Rutgersson, A. and Sterl, A. (2011) A global view on the wind sea and swell climate and variability from ERA-40. *Journal of Climate*, 24(5), 1461–1479. https://doi.org/10.1175/2010JCLI3718.1.

Semedo, A., Vettor, R., Breivik, Ø., Sterl, A., Reistad, M., Soares, C. G. and Lima, D.C.A. (2015) The Wind Sea and swell waves climate in the Nordic seas. *Ocean Dynamics*, 65(2), 223–240. https://doi.org/10.1007/s10236-014-0788-4.

Sen, P. (1968) Estimates of the regression coefficient based on Kendall's tau. *Journal of the American Statistical Association*, 63, 1379–1389.

Theil, H. (1950) A rank-invariant method of linear and polynomial regression analysis. I, II and III. *Proceedings of the Royal Netherlands Academy of Sciences*, 53, 386–392 521–525, 1397–1412.

Unden, P., et al. 2002. Hirlam-5 scientific documentation. Tech. Rep. GKSS 97/E/46, SMHI, SMHI, SE-601 76 Norrkoping, Sweden.

Uppala, S., P. Kållberg, A. Simmons, and Coauthors, 2005: The ERA-40 re-analysis. *Quarterly Journal of the Royal Meteorological Society*, 131, 2961–3012. https://doi.org/10.1256/qj.04.176.

Wang, X., Y. Feng, and V. Swail, 2012: North Atlantic wave height trends as reconstructed from the 20th century reanalysis. *Geophysical Research Letters*, 39, L18 705, 6. https://doi.org/10.1029/2012GL053381.

Waseda, T., Webb, A., Sato, K., Inoue, J., Kohout, A., Penrose, B. and Penrose, S. (2018) Correlated increase of High Ocean waves and winds in the ice-free waters of the Arctic Ocean. *Scientific Reports*, 8(4489), 9. https://doi.org/10.1038/s41598-018-22500-9.

Weisse, R. and Günther, H. (2007) Wave climate and long-term changes for the southern North Sea obtained from a high-resolution hindcast 1958–2002. *Ocean Dynamics*, 57(3), 161–172. https://doi.org/10.1007/s10236-006-0094-x.

Weisse, R. and von Storch, H. (2010) *Marine Climate and Climate Change: Storms, Wind Waves and Storm Surges*. Berlin, Germany: Springer Science & Business Media, p. 219.

Yang, X. (2005) Background blending using an incremental spatial filter. *Hirlam Newsletter*, 49, 3–11.

Zong, Z. (Ed.). (2006) *Information-Theoretic Methods for Estimating of Complicated Probability Distributions*. Amsterdam, Netherlands: Elsevier Science, p. 298.

How to cite this article: Haakenstad H, Breivik Ø, Reistad M, Aarnes OJ. NORA10EI: A revised regional atmosphere-wave hindcast for the North Sea, the Norwegian Sea and the Barents Sea. *Int J Climatol*. 2020;1–27. https://doi.org/10.1002/joc.6458

APPENDIX

Offshore observations

Among the observation locations indicated in Figure 1, the stations 1–8 are offshore stations. Offshore stations typically observe winds at heights between 30 and 130 m. This adds uncertainty to the comparison to modelled 10-m wind speed. Observations in the North Sea and the Norwegian Sea are usually reduced to 10 m height along a power-law profile (Furevik and Haakenstad, 2012),

$$U(z) = U_{10}\left(\frac{z}{z_r}\right)^{\alpha}, \tag{A1}$$

where U_{10} is the wind speed at the reference height $z_r = 10$ m, and z is the observation height. It is customary to assume $\alpha = 0.13$, but it typically varies between 0.08 and 0.14 (Hsu *et al.*, 1994), and $\alpha = 0.08$ is normally a better fit over the ocean (Furevik and Haakenstad, 2012). We have instead chosen the NORSOK profile (NORSOK, 2007),

$$U(z) = U_{10}\left(1 + C\ln\frac{z}{z_r}\right) \tag{A2}$$

where $C = 5.73 \times 10^{-2}(1+0.15U_{10})^{1/2}$, as it was found by Furevik and Haakenstad (2012) to give a better match than the power law profile (A1). It is however more expensive as it involves a third-order polynomial which requires an iterative root-finding procedure for the reduction to 10 m height.

Polar lows

It is of interest to qualitatively explore the development of polar lows in the two data sets to further assess the impact of changing the boundary conditions from ERA-40 to ERA-Interim. Polar lows are short-lived (less than 48 hr) meso-scale cyclones that are hard for numerical weather prediction models to capture (Rasmussen and Turner, 2003). It is known that NORA10 tends to underestimate the intensity of polar lows in the ERA-40 period (up to September 2002), and the lows typically do not continue to develop from one cycle to another (Haakenstad *et al.*, 2012). We will therefore first investigate if NORA10EI has an improved representation of polar lows compared to NORA10 forced by ERA-40 (before September 2002), and if the opposite is the case after August 2002.

Here, we have chosen to study four polar lows which evolve differently in NORA10 and NORA10EI. Two of the polar lows occur in the Barents Sea and two in the Norwegian Sea.

ERA-40 period: Polar low case 1 (January 12, 2002)

Figure A1 shows the track of the January 12, 2002 Barents Sea polar low and the NOAA image of the cloud signature. The polar low was first observed in position 74°N and 28°E. It moved south–east and dissolved after 15 hr hitting Novaya Zemlya. Figure A2 shows the evolution of the mean sea level pressure field in NORA10 and in NORA10EI and near-surface wind speed exceeding 14 $m \cdot s^{-1}$ from NORA10EI. The polar low is well

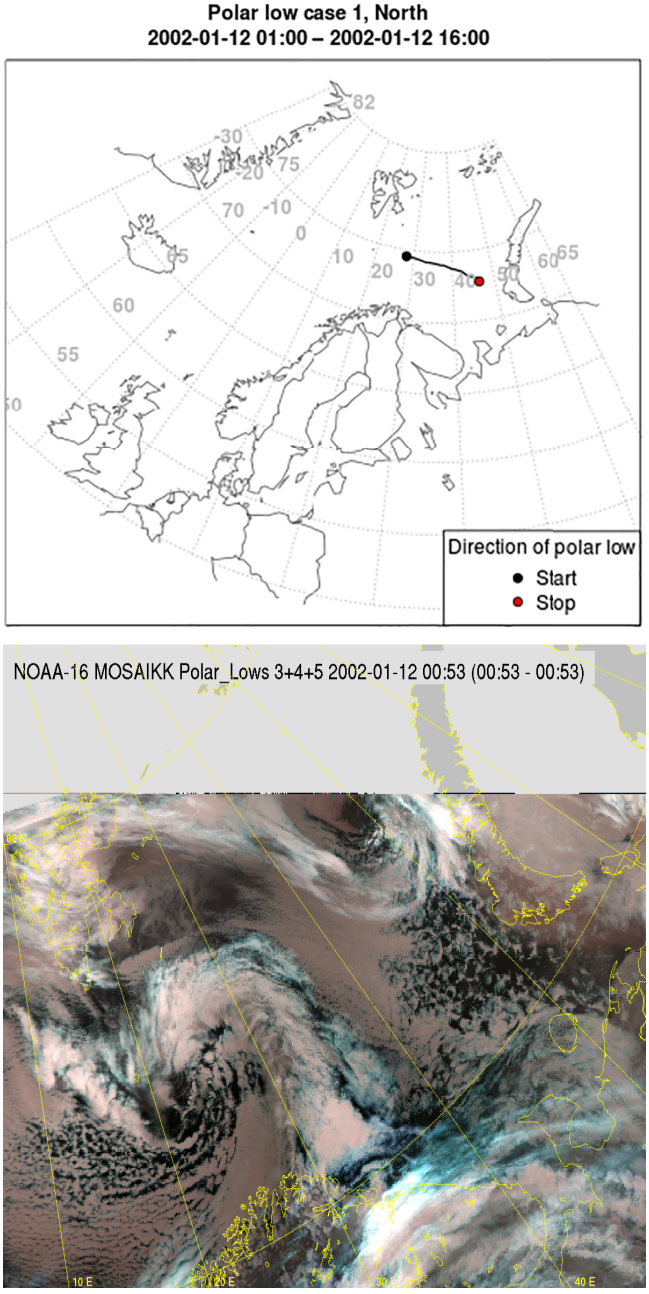

FIGURE A1 Track and NOAA-image of polar low January 12, 2002. Source: STARS database [Colour figure can be viewed at wileyonlinelibrary.com]

represented in NORA10EI. The cyclone has a mean sea level pressure of 980 hPa in the first-time step which decreases to 976 hPa after 13 hr. The maximum wind speed increases from 18 $m \cdot s^{-1}$ in the first-time step to 24 $m \cdot s^{-1}$ after 13 hr. NORA10 does not produce a cyclone until 5 hr later than observed and has a minimum mean

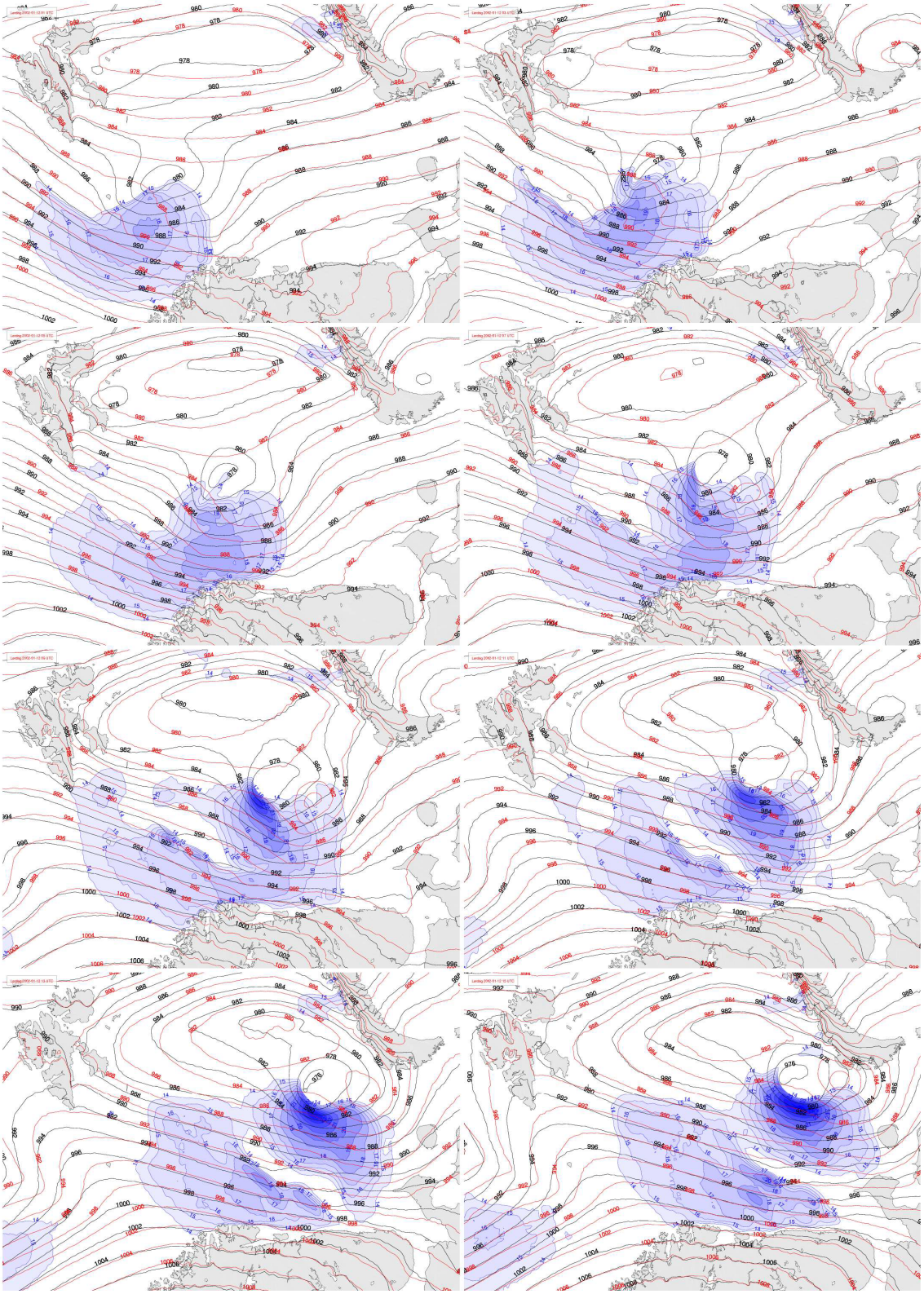

FIGURE A2 Polar low case January 12, 2002. Mean sea level pressure from NORA10EI (black) and NORA10 (red) and wind speed exceeding 14 $m \cdot s^{-1}$ from NORA10EI (blue) [Colour figure can be viewed at wileyonlinelibrary.com]

sea level pressure of 982 hPa. Maximum wind speed in NORA10 is 16 $m \cdot s^{-1}$. The conclusion from this polar low is that NORA10EI reproduces the polar low very well, while NORA10 shows a too late and too weak evolution.

ERA-40 period: Polar low case 2 (March 9, 2002)

Figure A3 shows the track of the March 9, 2002 Jan Mayen polar low and the NOAA-image of the cloud signature. The cloud image shows a characteristic comma-shaped pattern which suggests a typical wave cyclone near occlusion (Douglas *et al.*, 1995). The polar low was first observed just south of Jan Mayen with the vortex position 70°N and 5°W at 11 UTC, 9 March 2002. The polar low moved southward to the final observed position 65.5°N and 1.5°W 22 hr later. Figure A4 shows the evolution of the mean sea level pressure field in NORA10 and in NORA10EI together with the near-surface wind speed exceeding 14 $m \cdot s^{-1}$ from NORA10EI. The polar low occurs in the rear of a synoptic scale cyclone hitting Trøndelag at the time step when the polar low was first observed. The polar low is not a fully developed vortex in neither NORA10 nor NORA10EI in the first-time step, but shows up in NORA10EI as a cyclone 6 hr later than first observed and last for the rest of the observed period. NORA10 shows a polar low 8 hr later than first observed and this polar low does only last for 3 hr. According to these two situations, NORA10EI shows an improved representation of the polar lows compared to NORA10.

After ERA-40: Polar low case 3 (January 7, 2009)

The third polar low investigated, occurred in the Barents Sea 7 January 2009 and lasted for 7 hr. SAR winds of above 25 $m \cdot s^{-1}$ were observed in the Barents Sea and part of the coast of Finnmark. At Banak airport located sheltered in the innermost part of the Porsanger fjord, wind speed of 13 $m \cdot s^{-1}$ and wind gust of 17 $m \cdot s^{-1}$ were observed. Figure A5 shows the track of the polar low and the NOAA image of the cloud signature. Figure A6 shows the evolution of the mean sea level pressure field in NORA10 and in NORA10EI and near-surface wind speed exceeding 14 $m \cdot s^{-1}$ from NORA10. The location of the polar low is the same in NORA10 and NORA10EI. The location fits quite well with the observed polar low, but is somewhat too far east of the observed one. The polar low is fully developed in NORA10 at 04:00 UTC and in NORA10EI 1 hr later. NORA10 shows a maximum wind speed of 26 $m \cdot s^{-1}$ which last for the whole period of the polar low. This wind speed values fits the SAR

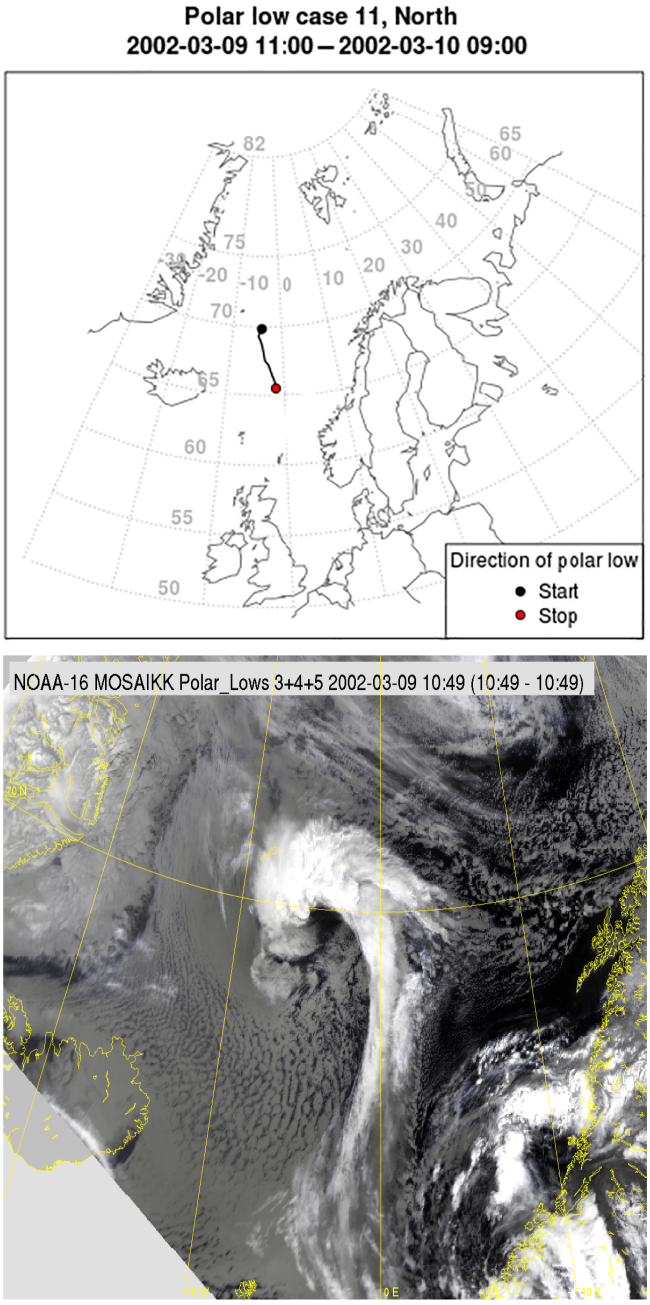

FIGURE A3 Track and NOAA-image of polar low March 9, 2002. Source: STARS database [Colour figure can be viewed at wileyonlinelibrary.com]

observations. NORA10EI shows somewhat lower wind speed and reaches 26 $m \cdot s^{-1}$ at just one-time step (2009-01-07 08:00).

After ERA-40: Polar low case 3 (7 January 2009)

The fourth polar low appeared in the Norwegian Sea at 18:00 UTC 26 February 2009 and lasted until 11:00 UTC 27 February. The Stars database[3] describes the polar low

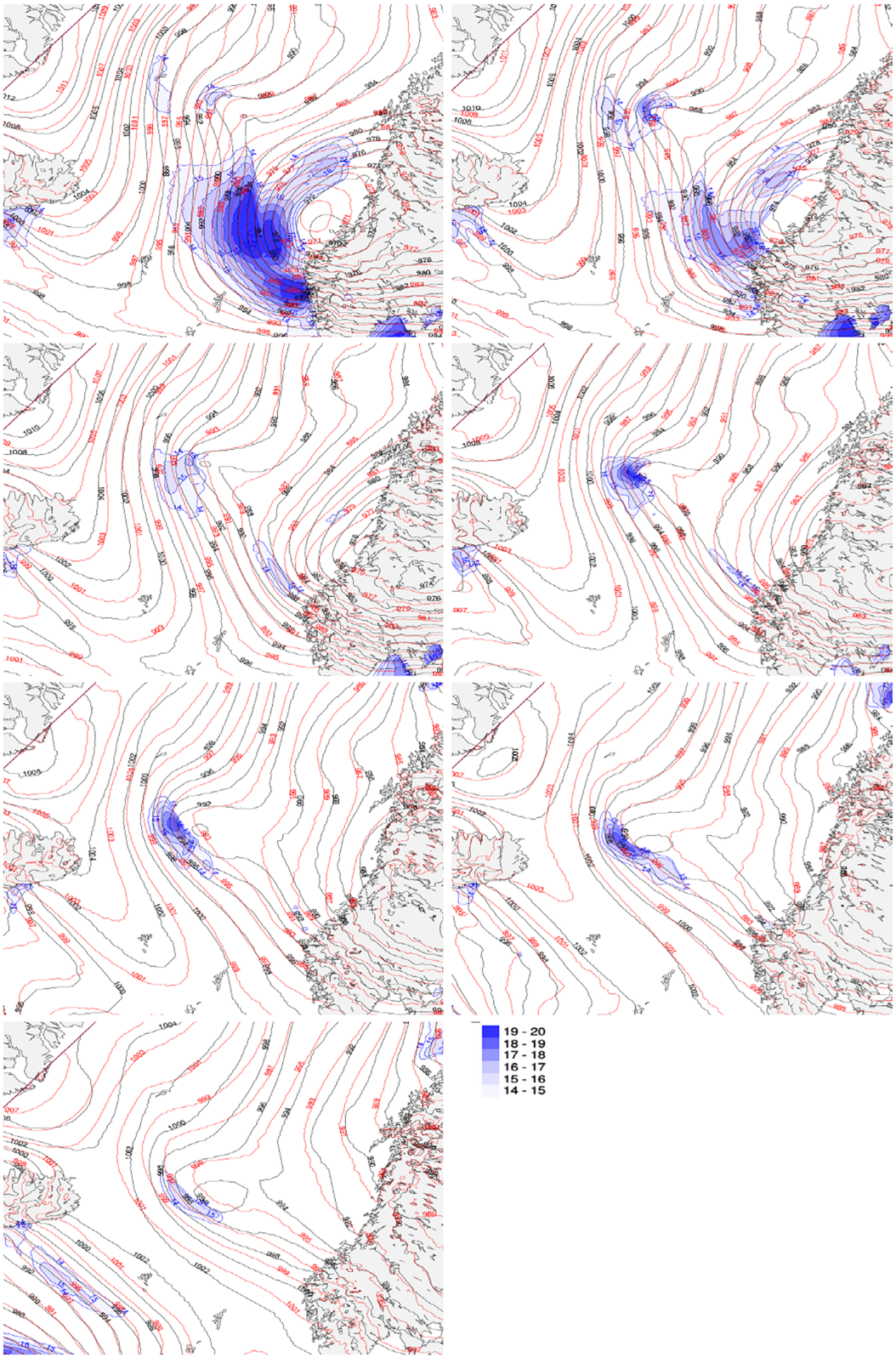

FIGURE A4 Polar low case March 9, 2002. Mean sea level pressure from NORA10EI (black) and NORA10 (red) and wind speed exceeding 14 m s^{-1} from NORA10EI (blue) [Colour figure can be viewed at wileyonlinelibrary.com]

as a classic version formed off the coast of Troms with a cold-air outbreak and a strong cold upper trough as precursors to the polar low. Southwest of the main low, a secondary, less intense centre formed. An inversion layer north east of the northern centre was broken by heating from air above the sea surface, intensifying the polar low.

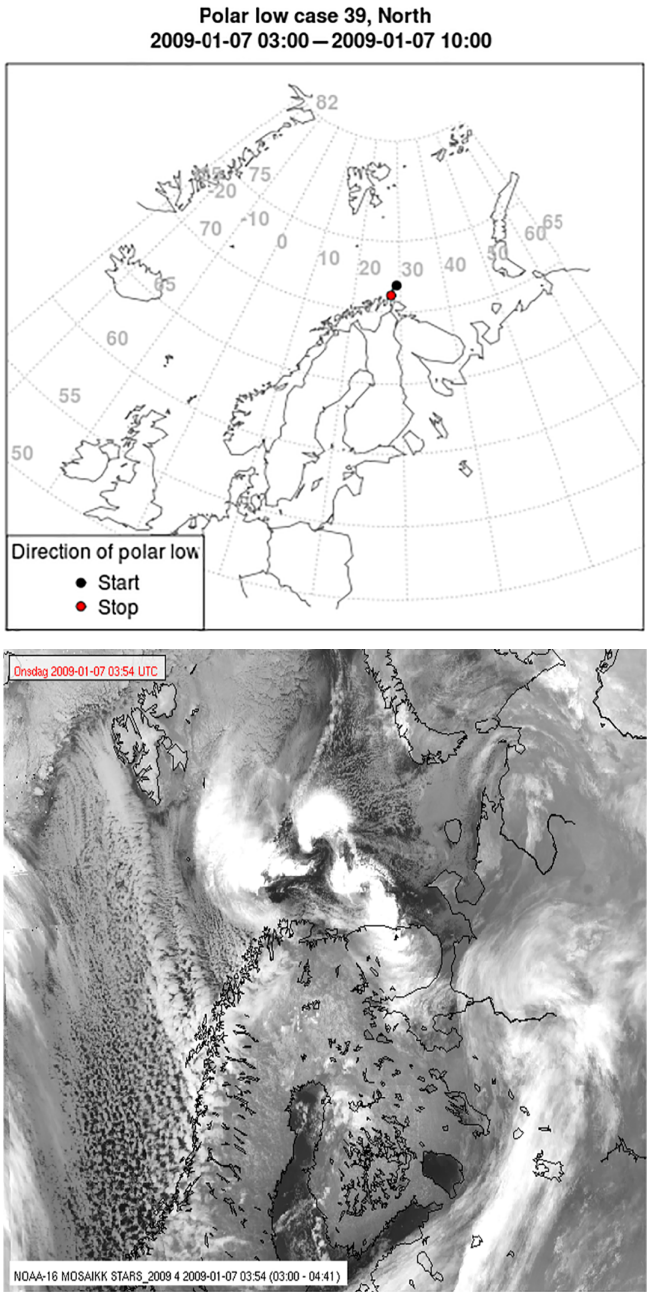

FIGURE A5 Track and NOAA-image of polar low January 7, 2009. Source: STARS database [Colour figure can be viewed at wileyonlinelibrary.com]

The low made landfall at the coast of the Nordland in northern Norway with a maximum observed wind speed of 23 $m \cdot s^{-1}$. Wind gusts up to 28 $m \cdot s^{-1}$ were observed. Figure A7 shows the track of the polar low and the NOAA-image of the cloud signature. Figure A8 shows that a polar low off the coast of Troms in northern Norway with a minimum mean sea level pressure of 989 hPa is present in both NORA10 and NORA10EI. However, the low is more extensive in NORA10 compared to NORA10EI. NORA10 shows the overall deepest mean sea level pressure throughout the lifetime of the low. NORA10 wind speed reached 24 $m \cdot s^{-1}$ at 02:00 UTC February 27, 2009, comparable, but slightly stronger than the NORA10EI wind speed (23 $m \cdot s^{-1}$). The maximum wind speeds in the models occur offshore and becomes strongly weakened before landfall.

Although no firm conclusions can be drawn from these four case studies, it seems clear that the polar lows are better represented by NORA10EI in the period up to September 2002 when ERA-40 was used as boundary conditions for NORA10, and conversely that NORA10 captures the polar lows better in the period after August 2002.

Trend analysis

The non-parametric Mann–Kendall (Mann, 1945; Kendall, 1975) and Sen's (Theil, 1950; Sen, 1968) method were used in the trend analysis of the 50th, 95th and 99th percentile wind speed in Section 6. The Mann–Kendall trend test is a frequently used test for monotonic trend in a time series based on Kendall rank correlation. The Mann–Kendall test statistic or score S is calculated as

$$S = \sum_{i=1}^{n-1} \sum_{j=i+1}^{n} \operatorname{sgn}(x_j - x_i) \tag{A3}$$

where n is the length of the time series, x is the data values in the time series, and sgn is the sign function;

$$\operatorname{sgn}(x_j - x_i) = \begin{cases} +1, & \text{if } x_j - x_i > 0 \\ 0, & \text{if } x_j - x_i = 0 \\ -1, & \text{if } x_j - x_i < 0. \end{cases} \tag{A4}$$

The variance is calculated as

$$\operatorname{var}(S) = \frac{n(n-1)(2n+5) - \sum_{i=1}^{m} t_i(t_i-1)(2t_i+5)}{18} \tag{A5}$$

where data having the same value in the sample, have been tied up in groups. m is the number of tied groups and t_i is the number of ties of extent i. With the requirement of a sample size which is greater than 10, the standard normal test statistic Z_s is computed as

$$Z_s = \begin{cases} \dfrac{S-1}{\sqrt{\operatorname{var}(S)}}, & \text{if } S > 0 \\ 0, & \text{if } S = 0 \\ \dfrac{S+1}{\sqrt{\operatorname{var}(S)}}, & \text{if } S < 0. \end{cases} \tag{A6}$$

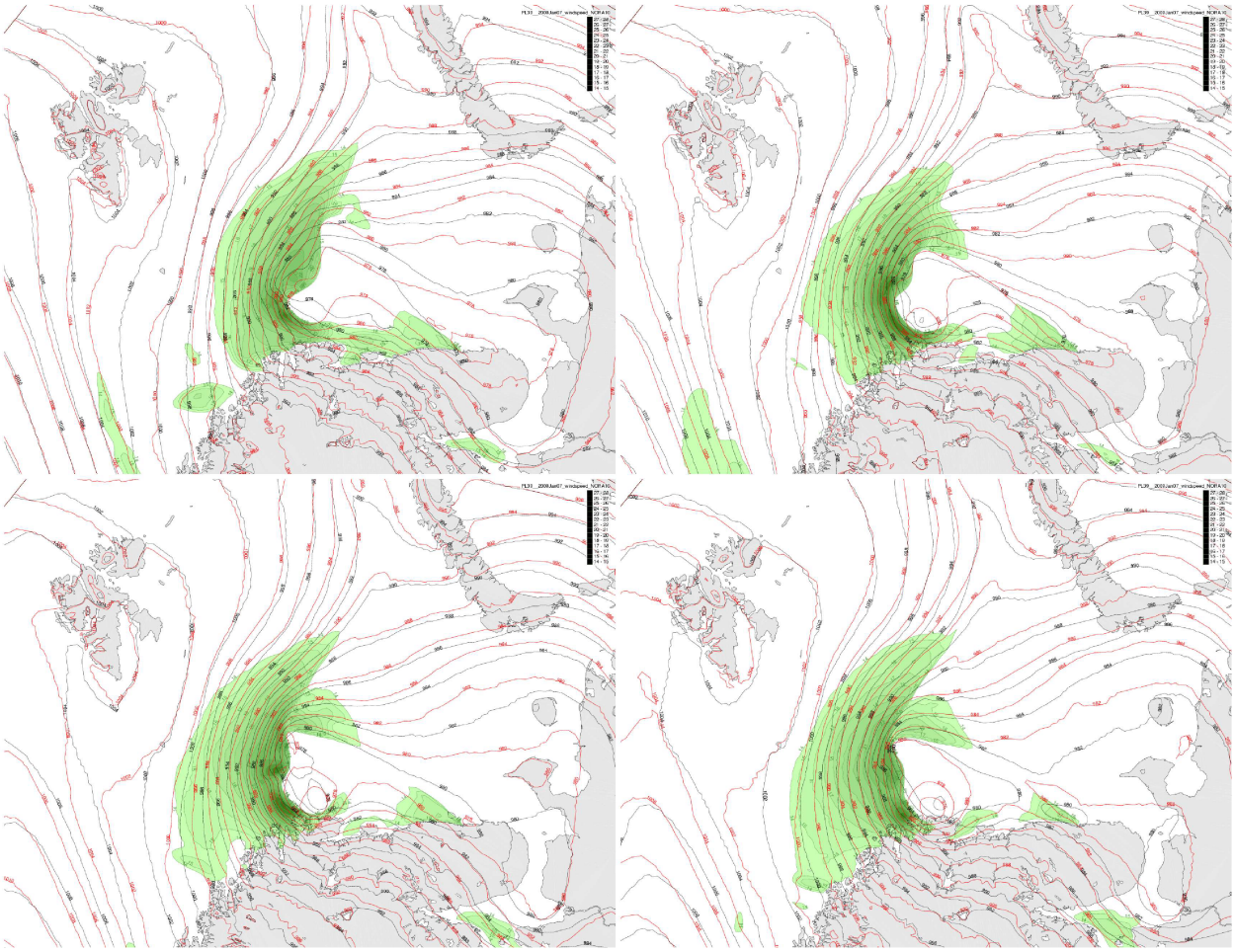

FIGURE A6 Polar low case January 7, 2009. Mean sea level pressure from NORA10EI (black) and NORA10 (red) and wind speed exceeding 14 m s^{-1} from NORA10 (green) [Colour figure can be viewed at wileyonlinelibrary.com]

If Z_s is positive, the trend is increasing and opposite, if Z_s is negative the trend is decreasing. The trend test is done at significance level $\alpha = 0.1$. Sen's slope is used to determine the strength of the trend, calculated as the median of the slopes in the time series,

$$Q_i = \text{median}\left(\frac{x_j - x_k}{j-k}\right). \tag{A7}$$

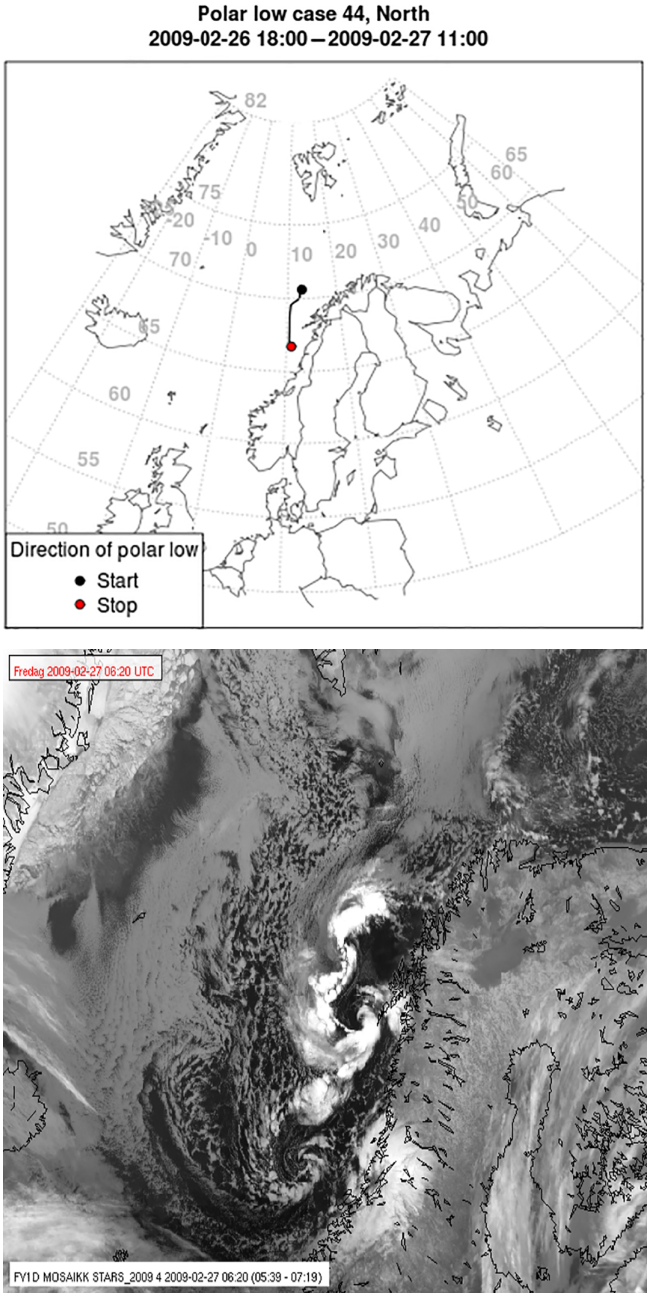

FIGURE A7 Track and NOAA-image of polar low February 26, 2009. Source: STARS database [Colour figure can be viewed at wileyonlinelibrary.com]

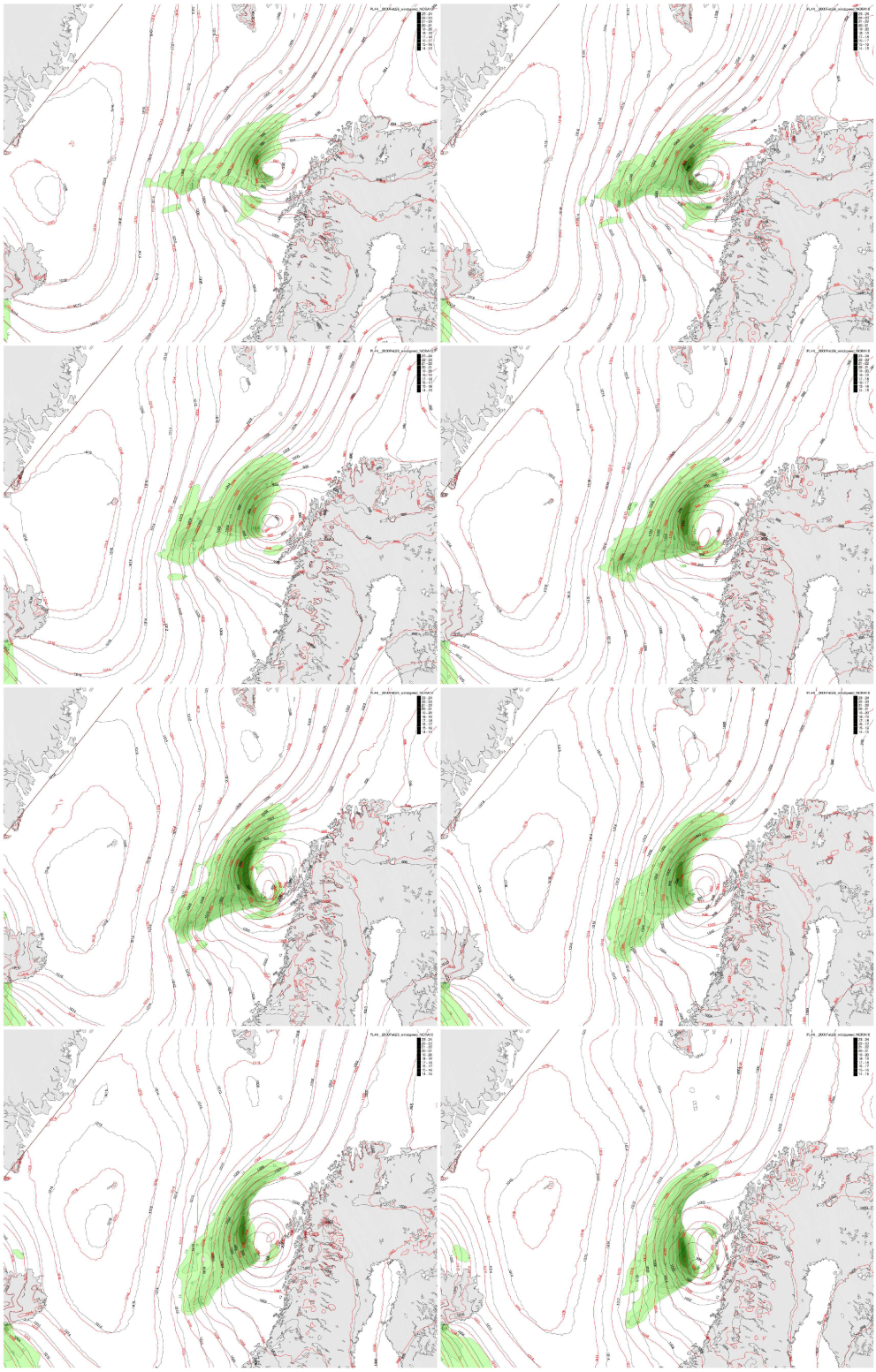

FIGURE A8 Polar low case 26 and February 27, 2009. Mean sea level pressure from NORA10EI (black) and NORA10 (red) and wind speed exceeding 14 m s^{-1} from NORA10 (green) [Colour figure can be viewed at wileyonlinelibrary.com]